Rock Mech Rock Eng
DOI 10.1007/s00603-013-0536-y

ORIGINAL PAPER

The Influence of NaCl Crystallization on the Long-Term Mechanical Behavior of Sandstone

Hong Zheng · Xia-Ting Feng · Quan Jiang

Received: 14 May 2013 / Accepted: 18 December 2013

Abstract Salt precipitation can occur in saline aquifers when the pore-fluid concentration exceeds saturation during carbon dioxide sequestration, especially in the dry-out region closest to the wellbore. Results from uniaxial and triaxial compression tests, creep tests, and poromechanical tests indicate that NaCl crystallization in pores enhances the compressive strength and bulk modulus under the given confining pressure, and reduces creep. In addition, it makes the pore liquid pressure in the sandstone less sensitive to changes in the hydrostatic stress under undrained conditions. A poro-viscoelastic model with crystals in the pores is proposed to quantitatively estimate the influence of in-pore NaCl crystallization on the long-term mechanical behavior of sandstone. By considering the thermodynamics of crystallization, a geometrical model of a crystal in a pore space is applied to the quasi-static equilibrium state of the crystallization. The solid–liquid interfacial energy is introduced to provide a convenient approach to couple the mechanical properties of sandstone (as a porous material) and the thermochemistry of the in-pore NaCl crystallization. By adding the solid–liquid interfacial energy, the Clausius–Duhem inequality for the skeleton is established for the viscoelasticity based on the proposed geometrical model of a crystal in the pore space. The constitutive equations are deduced from the free energy balance relationship to evaluate the influence of crystallization on the effective stress in terms of the solid–liquid interfacial energies and the pore-size distribution. By comparing the model's output with the test results, it is found that the poro-viscoelastic model describes the influence of in-pore NaCl crystallization on the long-term mechanical behavior of the sandstone reasonably well.

Keywords NaCl crystallization · Sandstone · Poro-viscoelasticity model · Interfacial energy · Long-term mechanical behavior

List of Symbols

A	Pore surface area (μm^2)
A^{e}	Elastic change of pore surface area (μm^2)
A^{v}	Viscous change of pore surface area (μm^2)
B	Skempton coefficient for sandstone without in-pore NaCl crystals
$B^{'}$	Skempton coefficient for sandstone with in-pore NaCl crystals
b_{ij}^{C}, b_{ij}^{L}	Crystal or liquid Biot's tangent tensor
b^{J}	Biot's coefficient scalars
C	Concentration of solution (mol/L)
C_0	Equilibrium solubility (mol/L)
C_{ijkl}	Tangent elastic stiffness modulus tensor of the rock skeleton
c	Mass fraction in NaCl solution
e_{ij}	Deviator strain tensor (MPa)
e_{ij}^{e}	Elastic deviator strain tensor
e_{ij}^{v}	Viscous deviator strain tensor
$\dot{e}_{ij}^{v}$	Viscous deviator strain rate tensor
F_D	Dissipation function
F_S	Helmholtz free energy of the skeleton (J)
G_s	Gibbs free energy (J)
G_0	Instantaneous shear modulus of the skeleton (MPa)
G_∞	Delayed shear modulus of the skeleton (MPa)

H. Zheng · X.-T. Feng (✉) · Q. Jiang
State Key Laboratory of Geomechanics and Geotechnical Engineering, Institute of Rock and Soil Mechanics, Chinese Academy of Sciences, Wuhan 430071, People's Republic of China
e-mail: xtfeng@whrsm.ac.cn; xia.ting.feng@gmail.com

Published online: 28 January 2014

K	Drained bulk modulus of sandstone without in-pore NaCl crystals (MPa)
$K^{'}$	Drained bulk modulus of sandstone with in-pore NaCl crystals (MPa)
K_{S}	Solid matrix bulk modulus of sandstone without in-pore NaCl crystals (MPa)
K_{S}'	Solid matrix bulk modulus of sandstone with in-pore NaCl crystals (MPa)
K_u	Bulk modulus of sandstone without in-pore NaCl crystals (MPa)
K_u'	Bulk modulus of sandstone with in-pore NaCl crystals (MPa)
K_0	Instantaneous bulk modulus of the skeleton (MPa)
K_∞	Delayed bulk modulus of the skeleton (MPa)
k	Permeability (dm)
L	Cylinder length of pore structure model (μm)
Δm	Pore liquid mass change (g)
N_{JK}	Biot's tangent modulus: subscript J or K standing for C (crystal) or L (liquid)
l, m, n	Cosine of θ_1, θ_2, θ_3 in Fig. 8
P_{C}	Crystal pressure (MPa)
P_{L}	Pore liquid pressure (MPa)
P_{S}	The total normal stress on cylinder pore surface (MPa)
Q_i	Normal row vector
Q_j	Normal column vector
R	Ideal gas constant (JK^{-1} mol^{-1})
R_{ij}	Pore stress distribution tensor
r_{p}	Average pore radius of pore structure model (μm)
r_{ca}	Pore canal radius (μm)
r_{th}	Pore throat radius (μm)
S_{s}	Entropy of the skeleton (JK^{-1})
S_{s}^0	Initial skeleton entropy (JK^{-1})
s_{ij}	Stress deviator tensor (MPa)
s_{ij}^0	Initial deviator stress (MPa)
T	Fahrenheit temperature (K)
T_0	Initial temperature (K)
t	Centigrade temperature (°C)
U	Viscous deformation energy (J)
$\dot{u}$	Deformation rate of the specimen in the creep test (ms^{-1})
V_i	Pore space position vector
v_{C}	Molar volume of a crystal (cm^3 mol^{-1})
W_{s}	Elastic work (J)
α	Skeleton thermal dilation coefficients scalars
α_1, α_2, α_3	Angles between $O^{'}A$ and the three projection axes $O^{'}\sigma_1'$, $O^{'}\sigma_2'$, $O^{'}\sigma_3'$ in Fig. 8
α_{ij}	Tangent thermal dilation coefficients tensor of the rock skeleton
$3\alpha_\varphi^{\mathrm{C}}$, $3\alpha_\varphi^{\mathrm{L}}$	Volumetric thermal dilation coefficient for crystal and liquid in pore
β	Ratio coefficient of viscous porosity variation
γ_{SL}, γ_{SC}, γ_{CL}	Liquid–solid, solid–crystal, crystal–liquid interfacial energy, respectively ($\mathrm{mJ/m}^2$)
γ_{SL}^0	Initial liquid–solid interfacial energy ($\mathrm{mJ/m}^2$)
δ	Thickness of the thin liquid film
δ_{ij}	Kronecker delta function
ε_{ij}	Strain tensor (MPa)
$\varepsilon_{ij}^{\mathrm{e}}$	Elastic part of strain tensor (MPa)
ε_{v}	Volumetric strain
$\varepsilon_{\mathrm{v}}^{\mathrm{e}}$	Elastic volumetric strain of the rock skeleton
$\varepsilon_{\mathrm{v}}^{\mathrm{v}}$	Viscous volumetric strain of the rock skeleton
$\dot{\varepsilon}_{\mathrm{v}}^{\mathrm{v}}$	Viscous volumetric strain rate of the rock skeleton
$\varepsilon_{\mathrm{vs}}^{\mathrm{v}}$	Viscous volumetric strain of the rock solid matrix
ς	Viscous shear modulus (MPa)
η	Coefficients of dissipation function
θ	Contact angle between crystal and pore surface (°)
θ_1, θ_2, θ_3	Angles between the principal stress coordinates and the vector $O'H$ in Fig. 8
κ	Viscous drained bulk modulus (MPa)
κ_{CL}	Curvature of crystal/liquid interface (1/μm)
ζ	Coefficients of dissipation function
σ_{c}, σ_l	Stress exerted on crystal or liquid by pore surface, $\sigma_{\mathrm{c}} + \sigma_l = P_{\mathrm{S}}$
σ_{ij}	Stress tensor (MPa)
σ_m	Hydrostatic (mean normal) stress (MPa)
σ_m^0	Initial mean stress (MPa)
σ_1, σ_2, σ_3	Major, intermediate, and minor principal stresses, respectively (MPa)
ϕ_1, ϕ_2, ϕ_3	Angles between the pore space position vector OO' and the three orthogonal principal stress axes in Fig. 8
φ	Porosity
φ^{e}	Elastic porosity variation
φ^{v}	Viscous porosity variation
φ_0	Initial porosity
φ_{C}, φ_{L}	Porosity occupied by crystal and liquid, respectively
$\varphi_{\mathrm{C}}^{\mathrm{e}}$, $\varphi_{\mathrm{L}}^{\mathrm{e}}$	Elastic change of porosity occupied by crystal and liquid, respectively
χ_{ij}	The deviator part of pore stress distribution tensor
χ	The product of deviator part of pore stress distribution tensor and pore stress distribution tensor $\chi = R_{ij}\chi_{ij}$

1 Introduction

In the process of carbon dioxide sequestration in saline aquifers, CO_2 can become trapped in the aquifer by dissolution in the water and by carbonization in rock minerals. Vaporization of water, as the result of the CO_2 dissolution and chemical reactions, will increase the concentration of salt in the pore fluid (Zeidouni et al. 2009). A special case is the dry-out region closest to the wellbore where freshly injected CO_2 may transport the vaporized water outwards thus causing an increased salt concentration in the pores. As a result of the high salinity of the brine, when the salt concentration exceeds its critical value, it causes precipitation of salt crystals in the pore fluid. This process not only affects pore properties but also exerts crystallization pressure on the reservoir rocks, which are porous. Crystallization pressure has an important influence on the mechanical properties of porous materials, which may lead to serious deterioration. For example, delayed ettringite formation may damage the mass concrete after hardening (Taylor et al. 2001) and salt crystallization may cause degradation of the porous sedimentary rocks used for building in coastal regions (Winkler and Singer 1972). Previous studies (Lewin 1982; Evans 1970) regarded salt crystallization in the pore spaces of such porous materials as a potential safety hazard. This is because it can damage or even destroy the porous material when the salt crystallization pressure exceeds the admissible value of the pore pressure. As the main component of the pore liquid in a saline aquifer is NaCl solution, and saline aquifers are long-term emission reservoirs for carbon dioxide, whether NaCl crystallization has a long-term effect on the mechanical properties of the reservoir's rocks needs to be investigated.

For NaCl crystallization in the pores of reservoir rocks, the driving force is related to supersaturation of the pore liquid depending on the solution concentration (Scherer 1999). Compared with a saturated solution, the solute in a corresponding supersaturated solution has a higher chemical potential. This excess chemical potential can bring to bear a crystallization pressure against an external restraint (Niels and Sadananda 2004). NaCl crystallization in pores thus changes the effective stress and the mechanical properties of the reservoir rocks because the crystals exert a pressure on the pore walls. Poromechanical and crystallization theories are attractive approaches to figuring out the acting mechanisms. Based on early poromechanical theory (Biot 1941; Cheng 1997; Coussy 1995); Wei and Muraleetharan (2002a, b) and Borja (2005) studied multi-phase, fluid-saturated or unsaturated porous media with a particular emphasis on the macroscopic properties and conservation equations in the pore fluid. Coussy (2007) later analyzed the role of freezing water as the crystal form playing a role in the poroelastic properties. However, the crystallization pressure of freezing water is determined by supercooling, while the determinant governing crystallization pressure in NaCl crystals is supersaturation, as well as the interfacial energies and pore size (Scherer 1999). In addition, Brice (2010) studied the influence of the stress field on the orientation of crystals growing in the pore network of an elastic porous medium with emphasis on the crystal shape under the far-field stress. The work, however, didn't include the effect of crystallization on the porous materials' mechanical constitution. According to the mechanism of in-pore crystallization, macroscopic deviatoric stress affects the in-pore crystallization orientation which, in turn, affects the mechanical properties of the porous material. Besides this, NaCl crystallization during the process of carbon dioxide sequestration in saline aquifers has been considered using a TOUGH2 simulator to figure out the evolution of the porosity and permeability of the reservoirs (Pruess and Spycher 2007). Nevertheless, this simulator is incapable of analyzing the effects of crystallization on the mechanical behavior of the reservoir rock material.

This paper investigates the influence of in-pore NaCl crystallization on the long-term mechanical behavior of the sandstone acting as the rock matrix of saline aquifers. Uniaxial and triaxial compressive tests, creep tests, and poromechanical tests have been conducted to investigate the effect of NaCl crystallization on the mechanical properties of sandstone (such as compressive strength, creep properties, and poromechanical properties). Based on poromechanical and crystallization theory, a viscoelastic model for the skeleton of the sandstone with crystallization in its pores is established. The Helmholtz free energy of the sandstone skeleton associated with the effect of NaCl crystallization in the pores, including crystallization pressure and surface free energy during material deformation, has been included in the viscoelastic constitutive model thus established. The parameters in the constitutive model of the sandstone skeleton are obtained from empirical formulae and the test results. The results indicate that the established model can capture the nature of the influence of in-pore NaCl crystallization on the long-term mechanical behavior of sandstone.

2 Experimental Methods

Three types of laboratory test have been used to investigate the influence of crystallization on the rock's mechanical behavior. The first involves uniaxial and triaxial compressive tests on sandstone specimens with and without in-pore NaCl crystallization to obtain the peak strength. This reflects the short-term mechanical properties of the sandstone with and without in-pore crystallization. The test results on peak strength are used to determine the axial

loading level of the creep test. Secondly, creep tests of sandstone specimens with and without in-pore NaCl crystallization have also been conducted to investigate the influence of in-pore NaCl crystallization on the long-term mechanical behavior of sandstone. Thirdly, poromechanical tests have been conducted to obtain the poromechanical parameters of sandstone specimens with and without in-pore NaCl crystal.

2.1 Preparation of the Sandstone Specimens

The sandstone specimens used in these three tests were sampled at the same location and have similar physical properties. The mean porosity of sandstone is 22.15 %. The specimens were prepared according to the methods suggested by the International Society for Rock Mechanics (ISRM) for uniaxial and triaxial compressive tests. To reduce the discreteness of the rock's physical and mechanical properties, specimens having wave velocities in the range of ±5 % of the average are accepted. The sizes, wave velocities, and saturation conditions of the specimens after oven-drying for 48 h at a temperature below 100 °C are shown in Table 1.

To obtain sandstone with in-pore NaCl crystallization, dry sandstone specimens are saturated with saturated NaCl solution at 30 °C using the vacuum suction method suggested by the ISRM. Since the solubility of NaCl increases with increasing temperature, this saturated solution will enter a supersaturated state at the test temperature of 25 °C. The difference in solubility of NaCl at 25 and 30 °C is 1.517 g/L and its supersaturation results in the formation and growth of NaCl crystals. Then, to maintain the same test temperature and minimize the effect of NaCl concentration on in-pore fluid properties, sandstone without in-pore NaCl crystallization is saturated with saturated NaCl solution at 25 °C as control experiments. In this way, at 25 °C, the sandstone specimens saturated with saturated NaCl solution consist of a solid skeleton and a crystal-free pore liquid while sandstone specimens saturated with an oversaturated NaCl solution consist of a solid skeleton, pore liquid, and pore crystals.

2.2 Uniaxial and Triaxial Compressive Strength Tests

Uniaxial and triaxial compressive tests on sandstone specimens with and without in-pore NaCl crystals were conducted using different confining pressures of 0, 10, 20, and 30 MPa, respectively. The specimen in the pressure cell is connected to the NaCl solution, in a sealed cavity, by tubes, which guaranteed supersaturation for NaCl crystal growth by the temperature difference between the pressure cell and the seal cavity. All tests were conducted isothermally at 25 °C. At least three specimens were used for each test. After the compressive tests, the failed specimens were drained of pore liquid using nitrogen to facilitate SEM and EDX processing. The results in Fig. 1 indicate that NaCl crystals exist in the sandstone saturated with supersaturated NaCl solution but the sandstone saturated with saturated NaCl solution was free of in-pore NaCl crystals. As seen in Fig. 2, at the same confining pressure, the average peak strength of the sandstone without in-pore NaCl crystals is lower than that with in-pore NaCl crystals. Furthermore, the linear Mohr–Coulomb envelope

Table 1 Size and wave velocities of the sandstone specimens

No.	Diameter (mm)	Height (mm)	Wave velocity (m/s)	Saturation condition of solution at 25 °C	No.	Diameter (mm)	Height (mm)	Wave velocity (m/s)	Saturation condition of solution at 25 °C
1	49.23	100.11	1,487	Saturation	17	49.20	100.20	1,487	Supersaturation
2	49.15	98.14	1,363	Saturation	18	49.22	100.08	1,433	Supersaturation
3	49.11	100.04	1,370	Saturation	19	49.04	100.10	1,375	Supersaturation
4	49.01	99.99	1,449	Saturation	20	49.02	100.20	1,378	Supersaturation
5	48.25	100.18	1,431	Saturation	21	49.18	99.96	1,489	Supersaturation
6	48.15	100.03	1,409	Saturation	22	48.32	100.08	1,419	Supersaturation
7	49.10	100.21	1,373	Saturation	23	48.10	100.18	1,377	Supersaturation
8	49.09	100.10	1,494	Saturation	24	49.12	99.96	1,494	Supersaturation
9	49.11	100.13	1,361	Saturation	25	49.14	100.52	1,399	Saturation
10	49.02	100.53	1,377	Saturation	26	49.10	99.72	1,434	Supersaturation
11	48.99	99.64	1,423	Saturation	27	49.06	99.58	1,387	Saturation
12	49.02	98.10	1,393	Saturation	28	49.00	99.80	1,493	Saturation
13	48.16	100.06	1,370	Supersaturation	29	49.20	99.70	1,426	Saturation
14	48.24	100.02	1,449	Supersaturation	30	49.25	99.91	1,486	Supersaturation
15	49.00	100.22	1,431	Supersaturation	31	48.99	99.94	1,415	Supersaturation
16	49.10	100.04	1,364	Supersaturation	32	49.15	100.02	1,394	Supersaturation

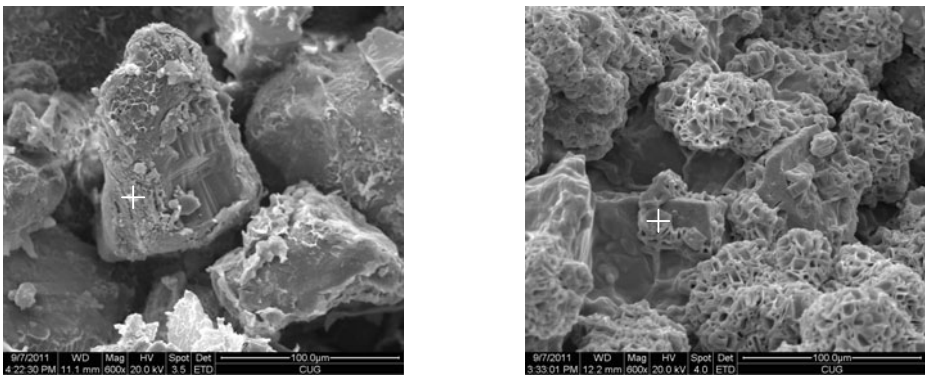

(a) (b)

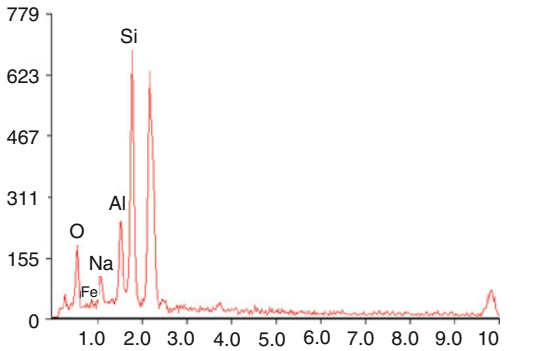

(c)

Element	Wt%	At%
O K	23.94	36.73
FeL	11.41	05.01
NaK	06.69	07.14
AlK	13.48	12.26
SiK	44.47	38.86

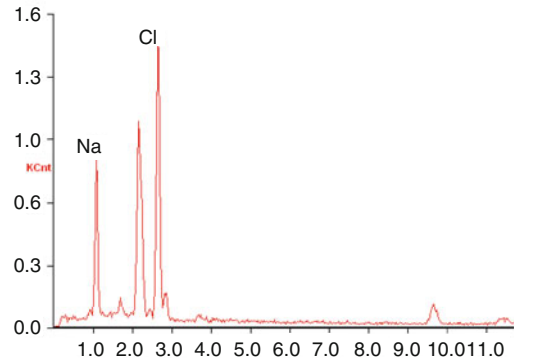

(d)

Element	Wt%	At%
NaK	34.68	45.02
ClK	65.32	54.98

Fig. 1 SEM pictures at 600 times magnification for **a** sandstone saturated with saturated NaCl solution, and **b** sandstone saturated with oversaturated NaCl solution after triaxial compressive tests, and **c** microanalysis result of EDAX on the surface point in (**a**), and **d** microanalysis result of EDAX on the crystals point in (**b**)

for sandstone with and without in-pore NaCl crystals is shown in Fig. 3: the apparent cohesion and angle of internal shearing resistance of sandstone without in-pore NaCl crystals are also lower than those with in-pore NaCl crystals. In other words, due to the improved "gluing effect" and attraction between the solid grains, in-pore NaCl crystallization increases the shear strength of the sandstone specimens.

2.3 Creep Properties of Sandstone with and Without In-Pore NaCl Crystals

To explore the effect of in-pore NaCl crystallization on the long-term mechanical behavior of sandstone, a series of isothermal creep tests under undrained conditions using 5 MPa confining pressure and three levels of deviator stress (10, 15, and 20 MPa) were conducted on specimens with and without in-pore crystals. The loading cell temperature was also controlled at 25 °C, i.e., the temperature at which the uniaxial and triaxial compressive tests were conducted. As in the compressive tests, the specimen in the pressure cell was also connected to the NaCl solution in a sealed cavity with inter-connecting tubes. Besides this, the solution in the seal cavity can be supplied using a pump during creep testing to provide the necessary supersaturation required for growth of in-pore NaCl crystals. At each deviator stress level, if the deformation rate is $\dot{u} \leq 10^{-7}$ m/s (Jun 1999), it can be considered that the specimen will reach its stable creep stage. Then, the next deviator stress level is loaded. As indicated in

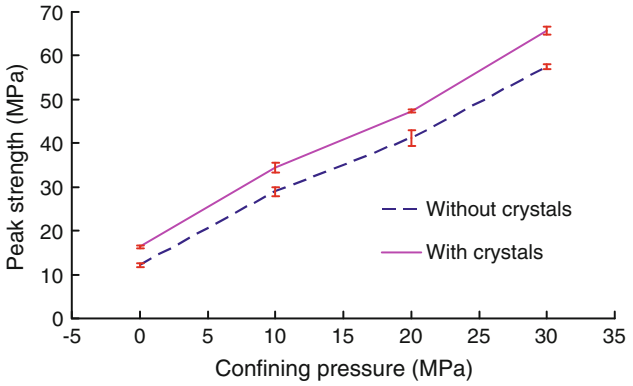

Fig. 2 The mean peak strength and confining pressure of sandstone with and without in-pore NaCl crystals

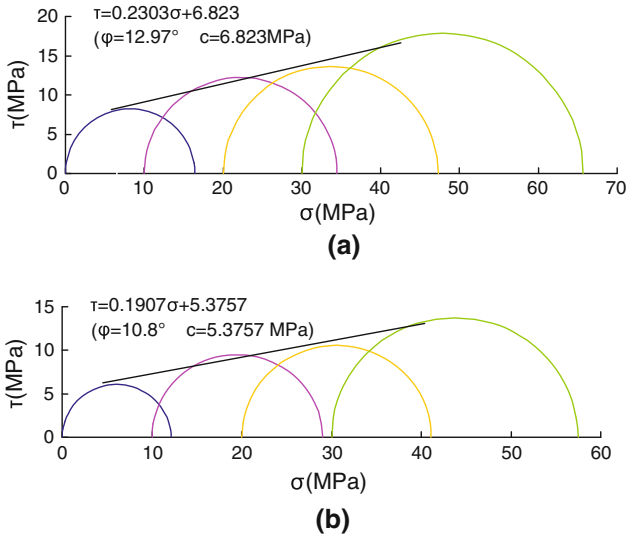

Fig. 3 The linear Mohr–Coulomb envelopes for **a** sandstone with in-pore NaCl crystals, and **b** sandstone without in-pore NaCl crystals

Fig. 4, there are NaCl crystals precipitated in the pores of the sandstone saturated with oversaturated NaCl solution while there are no NaCl crystals adhering to the surface of the mineral particles in sandstone saturated with saturated NaCl solution. As can be seen from Fig. 5, the difference between initial and final values of the axial strain during each creep level and the time taken to reach stable creep in the sandstone without in-pore NaCl crystals are larger than those for sandstone with in-pore NaCl crystals. This means that in-pore NaCl crystallization reduces creep.

2.4 Poromechanical Parameters of Sandstone with and Without In-Pore NaCl Crystals

In order to investigate the effect of NaCl crystallization on the poromechanical properties of sandstone with and without in-pore NaCl crystals, three kinds of isothermal isotropic compression tests were conducted. The loading cell temperature was also controlled at the same 25 °C as before. The test results are summarized in Table 2.

(1) Undrained isotropic compression tests (UHP)

The sandstone specimens with and without in-pore NaCl crystals were loaded under undrained conditions. All tests had the same loading path process, i.e., the axial stress and confining pressure was increased up to 10 MPa at the same loading rate and in the same stress state keeping $\sigma_1 = \sigma_2 = \sigma_3 = \sigma_m$. Curves showing the pore liquid pressure and hydrostatic stress and curves of the hydrostatic stress and volumetric strain for specimens with and without in-pore NaCl crystals were thus obtained, as shown in Fig. 6. Skempton coefficients, B′ and B, for the sandstone with and without in-pore NaCl crystals, respectively, can be obtained by calculating $B = -\frac{\Delta P_L}{\Delta \sigma_m}$. The bulk moduli K'_u and K_u for both cases can also be obtained using $K_u = \left[\frac{\Delta \sigma_m}{\Delta \varepsilon_v}\right]_{\Delta m=0}$, where the pore liquid mass is unchanged (i.e., $\Delta m = 0$).

(2) Drained isotropic compression tests (DHP)

The sandstone specimens with and without in-pore NaCl crystals had the same loading process here as in the UHP tests but without the pore liquid pressure increment. The drained bulk modulus K' and K for the sandstone with and without in-pore NaCl crystals can be obtained from Fig. 7a by using the formula $K = \left[\frac{\Delta \sigma_m}{\Delta \varepsilon_v}\right]_{\Delta P_L=0}$, where the pore liquid pressure is invariant (i.e., $\Delta P_L = 0$).

(3) Uniform loading rate tests (ULR)

Hydrostatic stress for the sandstone specimens with and without in-pore NaCl crystals followed the same loading process as UHP tests. Meanwhile, pore pressure was increased at the same rate as the hydrostatic stress during these tests. The solid matrix bulk modulus, K_S and K'_S, are calculated from the curves in Fig. 7b by using the formula $K_S = \left[\frac{\Delta \sigma_m}{\Delta \varepsilon_v}\right]_{\Delta \sigma_m=\Delta P_L}$.

Table 2 shows the different poromechanical parameters of the sandstones with and without in-pore NaCl crystals. All the poromechanical parameters of the sandstones with in-pore NaCl crystals, except the Skempton coefficient, are larger than those without crystals. Due to the NaCl crystallization in the pores, solid cementation of the sandstones with in-pore NaCl crystals is enhanced and its bulk modulus then improved. Skempton coefficients are poromechanical parameters reflecting pore compressibility. As a result of the smaller porosity and poorer pore connectivity in sandstones with in-pore NaCl crystals (due to the crystals filling and cementing the pores), its Skempton coefficient is smaller than in sandstone without crystals. Besides, the skeleton of sandstones with in-pore NaCl crystals is

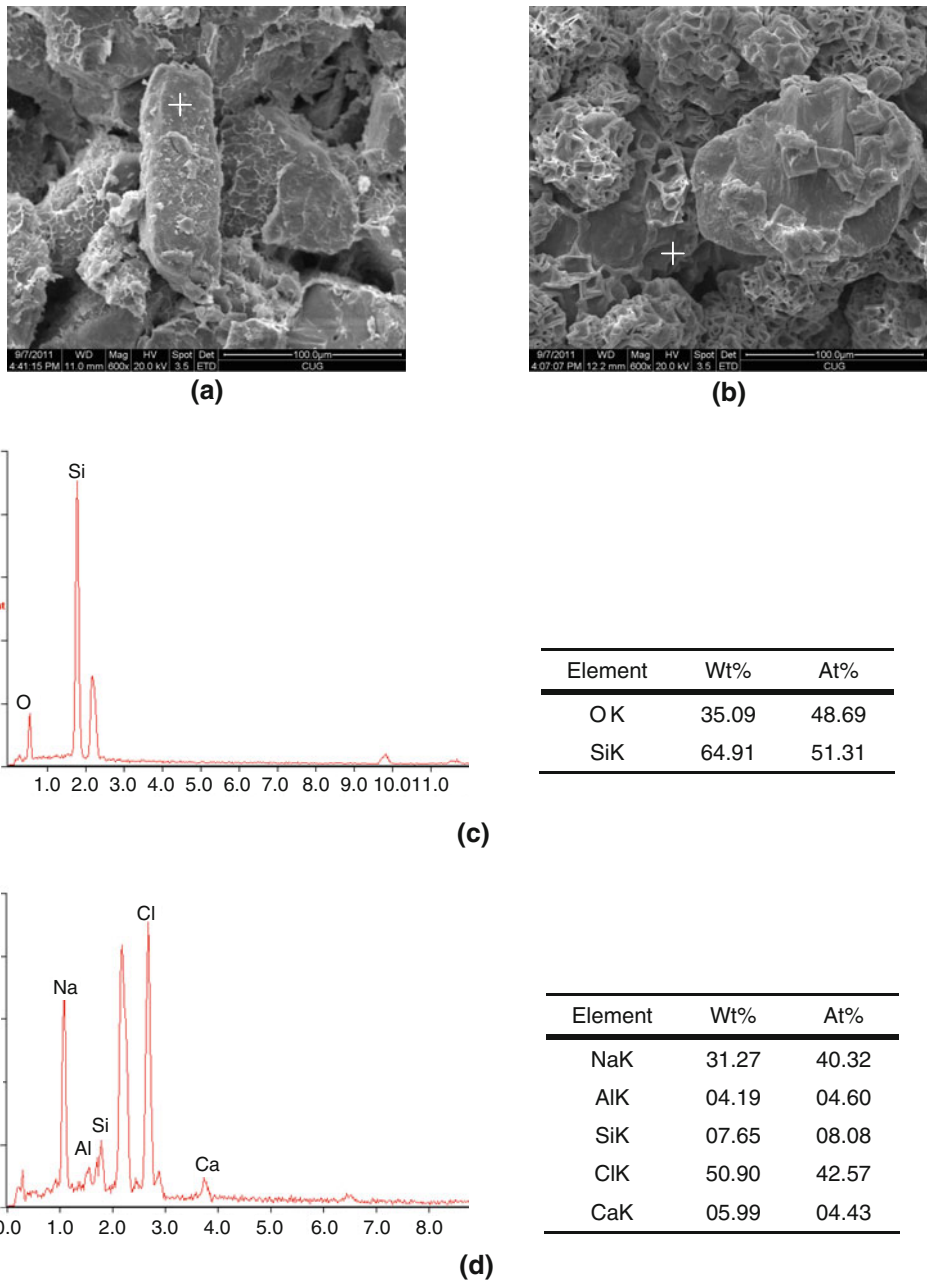

Element	Wt%	At%
O K	35.09	48.69
SiK	64.91	51.31

Element	Wt%	At%
NaK	31.27	40.32
AlK	04.19	04.60
SiK	07.65	08.08
ClK	50.90	42.57
CaK	05.99	04.43

Fig. 4 SEM pictures at 600 times magnification for **a** sandstone saturated with saturated NaCl solution, and **b** oversaturated NaCl solution after the creep tests, and **c** microanalysis result of EDAX on the surface point in (**a**), and **d** microanalysis result of EDAX on the surface point in (**b**)

harder than these without crystals, which makes the specimens less compressible.

The results of the compressive tests, creep tests, and poromechanical tests indicate that NaCl crystallization in the pores can enhance the compressive strength and bulk modulus under a given confining pressure. It can also mask the creep characteristics (such as the difference between initial and final value of axial strain during each creep level and the time taken to reach stable creep) of the sandstone. Further, it also makes the pore liquid pressure in the sandstone less sensitive to the hydrostatic stress.

3 Viscoelasticity Model for Porous Materials with Crystallization

Based on thermochemistry and poromechanics, a viscoelastic mechanical model for porous materials with NaCl crystallization in pores is established to describe the long-term mechanical behavior of sandstone with NaCl crystallization. For a sandstone skeleton, taking the interfacial energy as the non-volume work in the laws of thermodynamics (Coussy 2004; Adamson 1990), the state equation for the rock skeleton can be expressed in a Clausius–Duhem inequality:

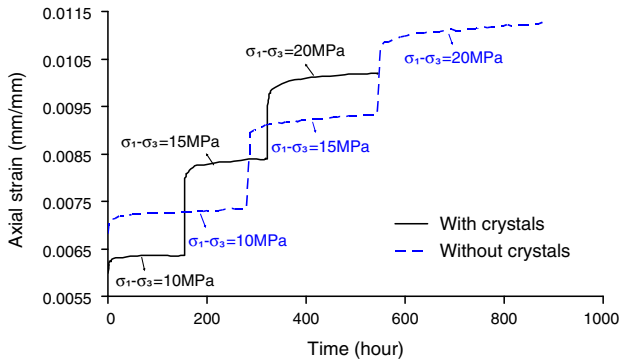

Fig. 5 Creep curves for sandstone without in-pore NaCl crystals and with in-pore NaCl crystals using confining pressure $\sigma_3 = 5$ MPa and three levels of deviator stress $\sigma_1 - \sigma_3 = 10$, 15, and 20 MPa, respectively

Table 2 Parameters in each hydrostatic stress test for sandstone specimens with and without in-pore NaCl crystals

Sandstone specimen	Components	Test type	Parameters
Without in-pore NaCl crystals	Solid matrix, pore liquid	UHP	$K_u = 1{,}970.29$ MPa; $B = 0.2681$
		DHP	$K = 1{,}526.20$ MPa
		ULR	$K_S = 10{,}151.30$ MPa
With in-pore NaCl crystals	Solid matrix, pore liquid, and pore crystal	UHP	$K'_u = 2{,}256.62$ MPa; $B' = 0.2086$
		DHP	$K' = 1{,}871.28$ MPa
		ULR	$K'_S = 11{,}365.21$ MPa

$$\sigma_{ij}\mathrm{d}\varepsilon_{ij} + P_C\mathrm{d}\,\varphi_C + P_L\mathrm{d}\,\varphi_L - S_s\mathrm{d}T + \gamma_{SL}\mathrm{d}A - \mathrm{d}F_s \geq 0, \quad (1)$$

where $\sigma_{ij}\mathrm{d}\varepsilon_{ij}$ is the infinitesimal element of strain work done by the surroundings on the entire porous material, P_C and P_L are the pressure in crystal and liquid. When the pore is filled by crystal and liquid, the porosity φ can be divided into partial φ_C and φ_L, which are occupied by crystal and liquid, respectively. S_s and T are the entropy of the skeleton and temperature, respectively. $\gamma_{SL}\mathrm{d}A$ is the infinitesimal interfacial energy increment at the fluid–solid interface with an infinitesimal area increment of the pore surface, and F_S is the Helmholtz free energy of the skeleton.

Here, compressive stress is defined as a positive quantity. The state equation includes the effect of the mechanical deformation of the porous solid on the part of the Helmholtz free energy associated with the evolution of the fluid–solid interface. The equality in Eq. 1 applies to elastic, i.e., reversible, processes.

In order to deduce the viscoelastic constitutive equations for the porous material with NaCl crystallization, the relationships between the parameters in the state equation, Eq. (1), are first investigated (Sect. 3.1). The relationship between the pore surface area A and the total porosity φ (including φ_L and φ_C) is established on the basis of a geometrical model which describes the equilibrium shape of the NaCl crystal and a cylindrical pore. The relationships between γ_{SL}, P_C, and P_L in the state equation are established by using crystal growth theory. P_S, the total normal stress on the pore surface, is introduced to describe the relation with P_L and the stress field σ_{ij} in the porous material. Based on these relations, the viscoelastic constitutive equations are then established in Sect. 3.2.

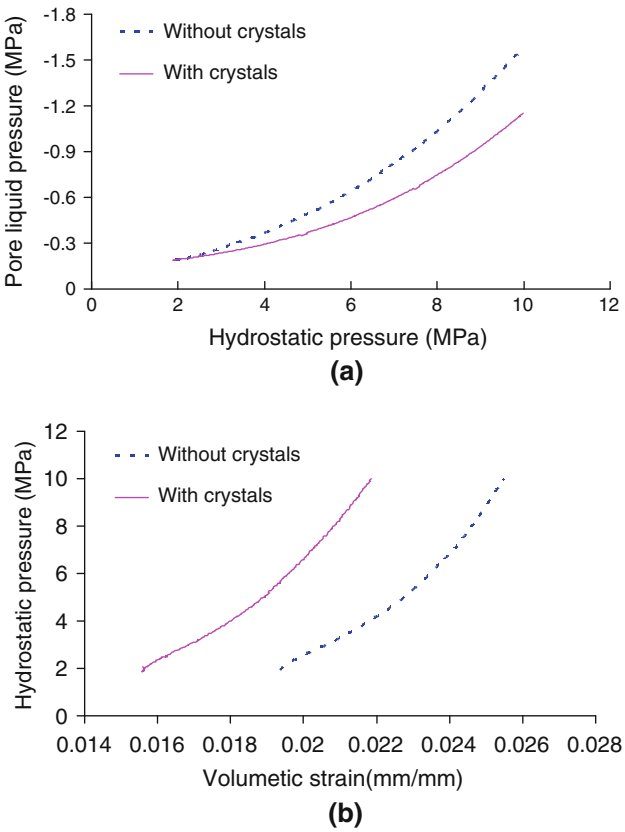

Fig. 6 **a** Pore liquid pressure (P_L) versus hydrostatic stress (σ_m), and **b** the hydrostatic stress (σ_m) versus volumetric strain (ε_v) of the sandstone specimens with and without in-pore NaCl crystals under undrained conditions

3.1 Determination of the Relationships Between Parameters

3.1.1 Determination of the Relationship Between A and φ

Porous materials are complex in terms of pore geometries, pore space position, and solid grain properties, etc. To quantify the pore geometry and connected space vector in the given space coordinate system, the pore network is described by an average pore radius r_p (Fig. 8) and a pore space position vector V_i (OO' in Fig. 8). A cylindrical pore structure model in each representative volume element is considered here (for uniformity just like the "tubes-in-series"

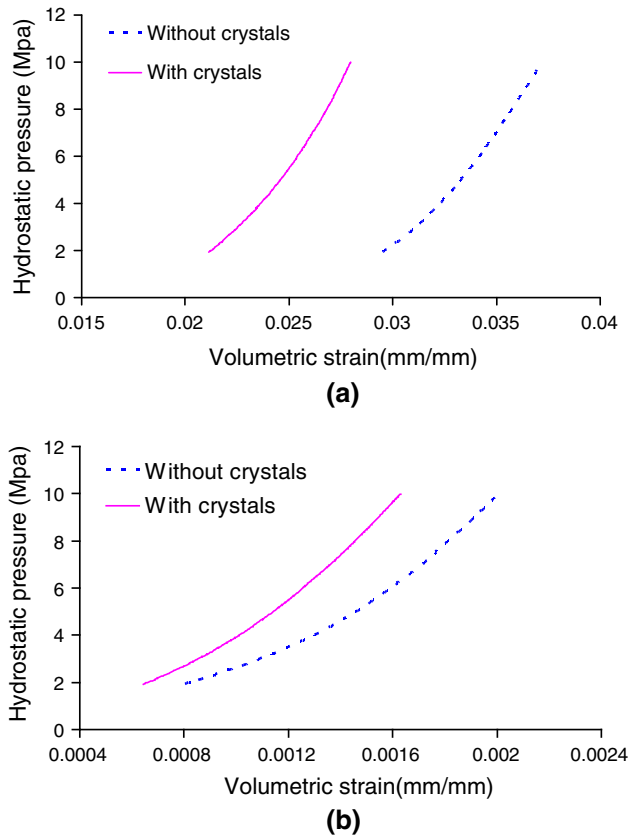

Fig. 7 **a** Hydrostatic pressure (σ_m) versus volumetric strain (ε_v) under drained conditions, and **b** hydrostatic pressure (σ_m) versus volumetric strain (ε_v) under the same loading rate of hydrostatic stress and pore pressure for the sandstone specimens with and without in-pore NaCl crystals

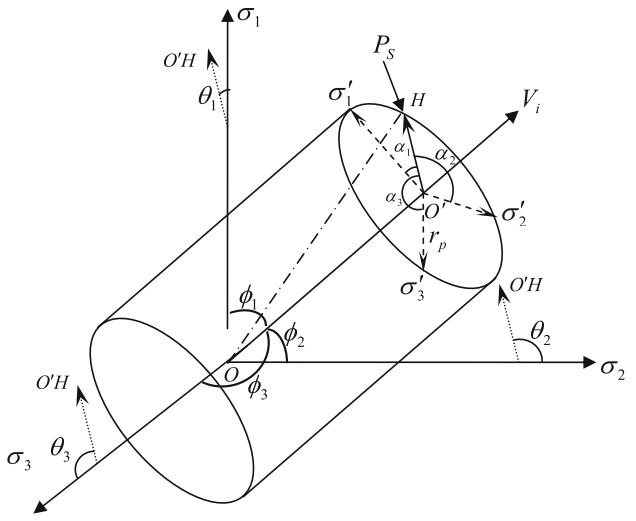

Fig. 8 Cylinder pore structure model for each representative volume element

model used in the TOUGH2 simulator for converging–diverging pore channels). The size of the cylinder pore model is specified to depend only on the average pore radius, r_p, while the cylinder length, L, is fixed as a constant. In each representative volume element, the cylindrical pore volume and surface area are expressed as $\varphi = Lr_p^2\pi$ and $A = 2Lr_p\pi$, respectively. The partial and total derivatives of φ with respect to A are given by

$$\frac{\partial\varphi}{\partial A} = \frac{r_p}{2}; \frac{d\varphi}{dA} = r_p. \tag{2}$$

As the pore shape includes the pore canal and pore throat described in the structure of reservoir rock for petroleum engineering, the average pore radius r_p can be obtained by calculating the average value of the pore canal radius r_{ca} and pore throat radius r_{th} using Eq. (3),

$$r_p = \frac{r_{ca} + r_{th}}{2}, \tag{3a}$$

where, r_{ca} and r_{th} are calculated by the following empirical formulae (Pittman 1992; Yang and Wei 2004):

$$\log r_{ca} = -0.117 + 0.475 \log k - 0.99 \log \varphi, \tag{3b}$$

$$r_{th} = \frac{20}{7}\sqrt{\frac{k}{\varphi}}. \tag{3c}$$

3.1.2 *Determination of the Relationship Between P_C and P_L*

To determine the relationship between P_C and P_L, the shape of the crystals in the pores is investigated. Similar in essence to the reverse mechanism of the pressure-solution at grain contact (Aharonov and Katsman 2009), the equilibrium shape of the crystal is formed by dissolution from the high pressure surfaces and precipitation at lower pressures. It is noted that, with the deformation of the porous matrix and change in the stress field, the equilibrium state is disturbed and a new equilibrium is established via ionic transportation. Compared with the long-term process of sandstone deformation, the relaxation time for ionic transportation to establish a new equilibrium is much shorter. Therefore, during long-term deformation of sandstone, the crystallization state can be considered as a quasi-static equilibrium state which satisfies the phase equilibrium of the solute between solution and crystal with equilibrium shape. In the quasi-static equilibrium state, the chemical potentials are equal everywhere along the crystal surface, and there is no phase change on the contact surface around the crystal. For crystals in pores, the equilibrium shape is restricted by the pore surface. In this case, the stress on the pore surface generated from crystallization depends on the crystal equilibrium shape and pore structure.

The crystallization pressure can be expressed in terms of solution activity (Scherer 1999; Flatt and Scherer 2008) as:

$$P_{\mathrm{C}} = P_{\mathrm{L}} + \frac{RT}{v_{\mathrm{C}}} \ln\left(\frac{a}{a_0}\right), \tag{4}$$

where R is the ideal gas constant, a is the activity of the solution, a_0 is the equilibrium activity of the solution, and v_{C} is the molar volume of the crystal.

According to Laplace's equation (Adamson 1990), an alternative formulation for crystallization pressure using γ_{CL} and κ_{CL} can be written as:

$$P_{\mathrm{C}} = P_{\mathrm{L}} + \gamma_{\mathrm{CL}}\kappa_{\mathrm{CL}}. \tag{5}$$

The interfacial energy and interface curvature are represented as:

$$\gamma_{\mathrm{CS}} = \gamma_{\mathrm{LS}} - \gamma_{\mathrm{CL}} \cos\theta, \tag{6a}$$

$$\kappa_{\mathrm{CL}} = -\frac{2\cos\theta}{r_{\mathrm{p}}}, \tag{6b}$$

where θ is the contact angle between the crystal and the pore surface shown in Fig. 9.

To investigate the effect of crystallization pressure on the mechanical behavior in the porous material, the maximum pressure in the crystal is suggested to be in the quasi-static equilibrium state, i.e., that at the contact angle $\theta = 180°$. In that case, a thin liquid film with thickness δ ($\delta \ll r_{\mathrm{p}}$) exists between the crystal and the pore surface, as shown in Fig. 10.

As Fig. 11 shows, along with the pressure in the crystal, the pressure in the liquid and the capillary pressure from the crystal-liquid surface, the mechanical equilibrium at the tip of the crystal can be established as:

$$P_{\mathrm{C}} = P_{\mathrm{L}} + \frac{2\gamma_{\mathrm{CL}}}{r_{\mathrm{p}} - \delta}. \tag{7}$$

Considering the pressure in the crystal, the pressure in the liquid, the stress exerted on the crystal's side by pore surface σ_{c}, and the capillary pressure from the crystal–liquid surface, the mechanical equilibrium at the cylindrical sides of the crystal can be established as:

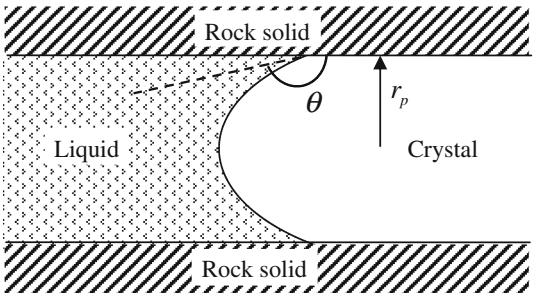

Fig. 9 Shape of a salt crystal in a cylindrical pore with radius r_{P}. The contact angle between the crystal and the pore wall is θ

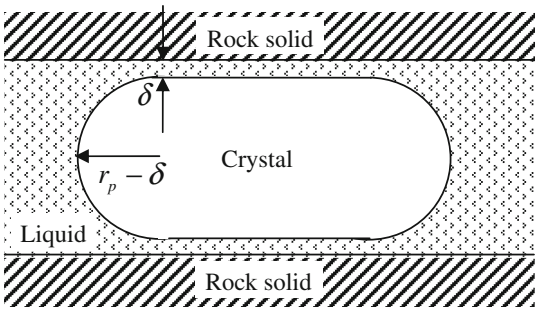

Fig. 10 Pore structure model of the porous material subjected to in-pore crystallization when a thin liquid film of thickness δ exists between the crystal and pore inner wall

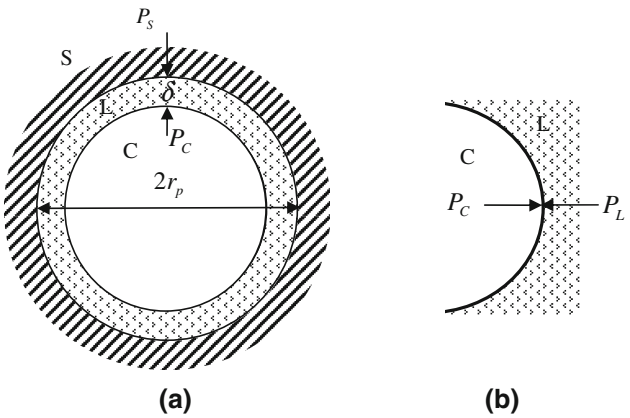

Fig. 11 **a** A cross-section of the surface of the pore structure, and **b** the tip of the crystal in the pore

$$P_{\mathrm{C}} = P_{\mathrm{L}} + \frac{\gamma_{\mathrm{CL}}}{r_{\mathrm{p}} - \delta} + \sigma_{\mathrm{c}}. \tag{8}$$

3.1.3 *Determination of the Relationship Between P_S, P_L, and σ_{ij}*

By considering contributions from σ_{c}, the pressure in the liquid, and the capillary pressure from the solid–liquid interface, the total normal stress on the cylinder pore surface can be expressed as:

$$P_{\mathrm{S}} = P_{\mathrm{L}} + \sigma_{\mathrm{c}} - \frac{\gamma_{\mathrm{SL}}}{r_{\mathrm{p}}}. \tag{9}$$

P_{S} is both exerted on the crystal and liquid and is related to the stress field in the rock.

According to the Cauchy formula, P_{S} at the random point H on the pore surface in Fig. 8 with the normal row vector Q_i and the normal column vector Q_j is defined as:

$$P_{\mathrm{S}} = Q_i \sigma_{ij} Q_j, \tag{10a}$$

$$Q_i = Q_j' = \overline{O'H} = (l, m, n), \tag{10b}$$

where Q_j' is the transposed matrix of Q_j. Other quantities are $l = \cos\theta_1 = \cos\alpha_1 \sin\phi_1$, $m = \cos\theta_2 = \cos\alpha_2 \sin\phi_2$,

$n = \cos\theta_3 = \cos\alpha_3 \sin\phi_3$, and ϕ_1, ϕ_2, and ϕ_3 are the angles between the pore space position vector OO' and the three orthogonal principal stress axes σ_1, σ_2, and σ_3, respectively. Also, θ_1, θ_2, and θ_3 are the angles between the principal stress coordinates and the vector $O'H$, and α_1, α_2, and α_3 are the angles between $O'A$ and the three projection axes $O'\sigma_1'$, $O'\sigma_2'$, and $O'\sigma_3'$, respectively.

According to the trigonometric function relations, if the pore space position vector (V_i) is given, α_1, α_2, and α_3 can be reduced to one independent variable. The partial derivative of P_S with respect to σ_{ij} in Eq. (10) is written as:

$$\frac{\partial P_S}{\partial \sigma_{ij}} = Q_j Q_i = \begin{pmatrix} l^2 & ml & nl \\ lm & m^2 & nm \\ nl & mn & n^2 \end{pmatrix}. \tag{11}$$

At a given pore space position case, P_S changes with the variation of the position of point H. On the basis of a small deformation assumption, the pore geometry keeps cylindrical and the stress distributes uniformly around the pore surface. Therefore, the integral average of the normal stress P_S is used:

$$P_S = \frac{1}{2\pi}\int_0^{2\pi} Q_i \sigma_{ij} Q_j \mathrm{d}\alpha_1 = \int_0^{2\pi} \frac{Q_j Q_i}{2\pi}\mathrm{d}\alpha_1 \sigma_{ij} = R_{ij}\sigma_{ij}, \tag{12}$$

where $R_{ij} = \int_0^{2\pi} \frac{Q_j Q_i}{2\pi}\mathrm{d}\alpha_1$ is defined as the pore stress distribution tensor.

3.2 Establishment of the Viscoelastic Constitutive Equations for the Porous Material

A viscoelastic model for the porous material with crystallization is established to describe the influence of crystallization on the long-term mechanical behavior on the basis of the Clausius–Duhem inequality, Eq. 1. The constitutive equations for the porous material with crystallization consist of an elastic model and a viscous model which are established in the following sub-sections, respectively.

3.2.1 Elastic Model of the Constitutive Equations for the Porous Material with Crystallization

To investigate the elastic constitutive equations for the porous material with crystallization, Eq. (1) representing the Helmholtz free energy is transformed into the Gibbs free energy G_s as:

$$G_s = F_s - P_C\varphi_C^e - P_L\varphi_L^e, \tag{13}$$

where $-P_C\varphi_C^e - P_L\varphi_L^e$ is the elastic expansion work resulting from the variation of the pore volume in the crystal and liquid.

Substituting Eq. (13) into Eq. (1) in the elastic phase gives

$$\sigma_{ij}\mathrm{d}\varepsilon_{ij}^e - \varphi_C^e \mathrm{d}P_C - \varphi_L^e \mathrm{d}P_L - S_s\mathrm{d}T + \gamma_{SL}\mathrm{d}A^e - \mathrm{d}G_s = 0. \tag{14}$$

As a function of ε_{ij}^e, P_C, P_L, T, and A^e, the partial differential forms of $G_s = G_s\left(\varepsilon_{ij}^e, P_C, P_L, T, A^e\right)$ in Eq. (14) are derived as:

$$\sigma_{ij} = \frac{\partial G_s}{\partial \varepsilon_{ij}};\ \varphi_C^e = -\frac{\partial G_s}{\partial P_C};\ \varphi_L^e = -\frac{\partial G_s}{\partial P_L};\ S_s = -\frac{\partial G_s}{\partial T};$$
$$\gamma_{SL} = \frac{\partial G_s}{\partial A^e}. \tag{15}$$

According to Eqs. (2), (9), and (12), the following relationships can be deduced from Eq. (15) (see "Appendix A") as:

$$\frac{\partial \sigma_{ij}}{\partial A^e} = \frac{\partial \gamma_{SL}}{\partial \varepsilon_{ij}^e} = -r_p R_{kl} C_{ijkl};\ \frac{\partial \sigma_{ij}}{\partial P_J} = -\frac{\partial \varphi_J^e}{\partial \varepsilon_{ij}^e} = -b_{ij}^J, \tag{16a}$$

$$\frac{\partial \varphi_J^e}{\partial T} = \frac{\partial S_s}{\partial P_J} = -3\alpha_\varphi^J;\ \frac{\partial \sigma_{ij}}{\partial T} = -\frac{\partial S_s}{\partial \varepsilon_{ij}^e} = -C_{ijkl}\alpha_{kl}, \tag{16b}$$

$$\frac{\partial S_s}{\partial A^e} = -\frac{\partial \gamma_{SL}}{\partial T} = -r_p R_{kl} C_{ijkl}\alpha_{ij};\ \frac{\partial \gamma_{SL}}{\partial A^e} = r_p^2 R_{ij} R_{kl} C_{ijkl}. \tag{16c}$$

On the basis of Eq. (16), the incremental forms of the elastic constitutive equations are represented by:

$$\begin{aligned}\mathrm{d}\sigma_{ij} &= \frac{\partial \sigma_{ij}}{\partial \varepsilon_{kl}^e}\mathrm{d}\varepsilon_{kl}^e + \frac{\partial \sigma_{ij}}{\partial P_C}\mathrm{d}P_C + \frac{\partial \sigma_{ij}}{\partial P_L}\mathrm{d}P_L + \frac{\partial \sigma_{ij}}{\partial T}\mathrm{d}T + \frac{\partial \sigma_{ij}}{\partial A^e}\mathrm{d}A^e \\ &= C_{ijkl}\mathrm{d}\varepsilon_{ij} - b_{ij}^C\mathrm{d}P_C - b_{ij}^L\mathrm{d}P_L - C_{ijkl}\alpha_{kl}\mathrm{d}T - r_p R_{kl} C_{ijkl}\mathrm{d}A^e,\end{aligned} \tag{17a}$$

$$\begin{aligned}\mathrm{d}\varphi^e &= \mathrm{d}\varphi_C^e + \mathrm{d}\varphi_L^e \\ &= \sum_{\substack{J=C,L \\ K=C,L}} \left(\frac{\partial \varphi_J^e}{\partial \varepsilon_{ij}^e}\mathrm{d}\varepsilon_{ij}^e + \frac{\partial \varphi_J^e}{\partial P_K}\mathrm{d}P_K + \frac{\partial \varphi_J^e}{\partial T}\mathrm{d}T + \frac{\partial \varphi_J^e}{\partial A^e}\mathrm{d}A^e\right) \\ &= \sum_{\substack{J=C,L \\ K=C,L}} \left(b_{ij}^J\mathrm{d}\varepsilon_{ij}^e + \frac{1}{N_{JK}}\mathrm{d}P_K - 3\alpha_\varphi^J\mathrm{d}T\right) + \frac{r_p}{2}\mathrm{d}A^e,\end{aligned} \tag{17b}$$

$$\begin{aligned}\mathrm{d}S_s &= \frac{\partial S_s}{\partial \varepsilon_{ij}^e}\mathrm{d}\varepsilon_{ij}^e + \frac{\partial S_s}{\partial P_C}\mathrm{d}P_C + \frac{\partial S_s}{\partial P_L}\mathrm{d}P_L + \frac{\partial S_s}{\partial T}\mathrm{d}T + \frac{\partial S_s}{\partial A^e}\mathrm{d}A^e \\ &= C_{ijkl}\alpha_{kl}\mathrm{d}\varepsilon_{ij}^e - 3\alpha_\varphi^C\mathrm{d}P_C - 3\alpha_\varphi^L\mathrm{d}P_L + \frac{C}{T}\mathrm{d}T \\ &\quad - r_p R_{kl} C_{ijkl}\alpha_{ij}\mathrm{d}A^e,\end{aligned} \tag{17c}$$

$$\begin{aligned}\mathrm{d}\gamma_{SL} &= \frac{\partial \gamma_{SL}}{\partial \varepsilon_{ij}^e}\mathrm{d}\varepsilon_{ij} + \frac{\partial \gamma_{SL}}{\partial P_C}\mathrm{d}P_C + \frac{\partial \gamma_{SL}}{\partial P_L}\mathrm{d}P_L + \frac{\partial \gamma_{SL}}{\partial T}\mathrm{d}T + \frac{\partial \gamma_{SL}}{\partial A^e}\mathrm{d}A^e \\ &= -r_p R_{kl} C_{ijkl}\mathrm{d}\varepsilon_{ij}^e - \frac{r_p}{2}\mathrm{d}P_L + r_p R_{kl} C_{ijkl}\alpha_{ij}\mathrm{d}T + r_p^2 R_{ij} R_{kl} C_{ijkl}\mathrm{d}A^e.\end{aligned} \tag{17d}$$

Restricting consideration to isothermal changes and materials with isotropic linear poroelasticities, the effect of temperature is removed and Biot's tensor b_{ij}^J is isotropic and makes no contribution to the deviator stress s_{ij}. Since the tangential properties are constant, substituting the total

derivatives of φ with respect to A in Eq. (2) allows the isothermal, isotropic linear poroelasticity constitutive equations to be deduced from Eq. (17) (see "Appendix B") as:

$$\sigma_m - \sigma_m^0 = K\varepsilon_\mathrm{v} - \left(b^\mathrm{C} + b^\mathrm{L}\right)\left(P_\mathrm{L} - P_\mathrm{L}^0\right) - K(\varphi - \varphi_0), \tag{18a}$$

$$s_{ij} - s_{ij}^0 = 2Ge_{ij} - \chi_{ij}(\varphi - \varphi_0), \tag{18b}$$

$$\frac{1}{2}(\varphi - \varphi_0) = \left(b^\mathrm{C} + b^\mathrm{L}\right)\varepsilon_\mathrm{v} + \left(P_\mathrm{L} - P_\mathrm{L}^0\right)\cdot\left[\frac{1}{N_\mathrm{LL}} + \frac{2}{N_\mathrm{LC}} + \frac{1}{N_\mathrm{CC}}\right], \tag{18c}$$

$$\gamma_\mathrm{SL} - \gamma_\mathrm{SL}^0 = -r_\mathrm{p}\left(K\varepsilon_\mathrm{v} + \chi_{ij}e_{ij}\right) - \frac{r_\mathrm{p}}{2}\left(P_\mathrm{L} - P_\mathrm{L}^0\right) + r_\mathrm{p}(K + \chi)(\varphi - \varphi_0), \tag{18d}$$

where σ_m^0, s_{ij}^0, φ_0, P_L^0 and γ_SL^0 stand for the initial mean stress, deviator stress, porosity, liquid pressure, and interfacial energy, respectively.

3.2.2 *Viscous Model of the Constitutive Equations for Porous Materials with Crystallization*

To establish the viscous constitutive equations for a porous material with crystallization under isothermal conditions, the viscous deformation energy (U) as an energy that is irrecoverable but not dissipated during instantaneous elastic unloading, is introduced. The viscous deformation energy is stored in the rock skeleton by the viscous strain of the rock skeleton $\varepsilon_{ij}^\mathrm{v}$, the viscous change of porosity φ^v, and the viscous change of pore surface area A^v, i.e., $U = U(\varepsilon_{ij}^\mathrm{v}, \varphi^\mathrm{v}, A^\mathrm{v})$.

To simplify the relationship between the viscous change in porosity φ^v and the viscous volumetric strain of the rock skeleton, $\varepsilon_\mathrm{v}^\mathrm{v}$, the relation suggested by Coussy (2004) is adopted, namely,

$$\varphi^\mathrm{v} = \beta\varepsilon_\mathrm{v}^\mathrm{v}, \tag{19}$$

where the coefficient of viscous porosity variation, β, is a number from 1 to φ_0. $\beta = 1$ applies to a solid matrix exhibiting volumetric strain only instantaneously (with zero viscous component), while $\beta = \varphi_0$ corresponds to the case where the solid matrix experiences a viscous volumetric strain, which is equal to that of the skeleton (i.e., $\varepsilon_\mathrm{v}^\mathrm{v} = \varepsilon_\mathrm{vs}^\mathrm{v}$).

On the basis of Eqs. (2) and (19), φ^v and A^v are all represented by $\varepsilon_\mathrm{v}^\mathrm{v}$. Therefore, the viscous deformation energy depends on $\varepsilon_\mathrm{v}^\mathrm{v}$ and the viscous deviatoric strain in the rock skeleton e_{ij}^v only, i.e., $U = U(\varepsilon_\mathrm{v}^\mathrm{v}, e_{ij}^\mathrm{v})$.

By introducing the viscous drained bulk modulus κ and the viscous shear modulus ς which are analogous to the drained bulk modulus K and the shear modulus G in the elastic work equation, the viscous deformation energy U can be defined, in a manner similar to the elastic deformation energy, by:

$$U(\varepsilon_\mathrm{v}^\mathrm{v}, e_{ij}^\mathrm{v}) = \frac{1}{2}\kappa\varepsilon_\mathrm{v}^{\mathrm{v}2} + \zeta e_{ij}^{\mathrm{v}^2}. \tag{20}$$

As the total strain ε_{ij} and porosity φ consist of the elastic components and viscosity components, respectively,

$$\varepsilon_{ij} = \varepsilon_{ij}^\mathrm{e} + \varepsilon_{ij}^\mathrm{v}, \tag{21a}$$

$$\varphi = \varphi^\mathrm{e} + \varphi^\mathrm{v}. \tag{21b}$$

The free energy of the rock skeleton, F_s, split into elastic work W_s and viscous energy U can thus be expressed as

$$F_\mathrm{s} = W_\mathrm{s}\left(\varepsilon_\mathrm{v}^\mathrm{e}, e_{ij}^\mathrm{e}, \varphi^\mathrm{e}, A^\mathrm{e}\right) + U\left(\varepsilon_\mathrm{v}^\mathrm{v}, e_{ij}^\mathrm{v}\right), \tag{22a}$$

$$W_\mathrm{s}\left(\varepsilon_\mathrm{v}^\mathrm{e}, e_{ij}^\mathrm{e}, \varphi^\mathrm{e}, A^\mathrm{e}\right) = W_\mathrm{s}\left(\varepsilon_\mathrm{v} - \varepsilon_\mathrm{v}^\mathrm{v}, e_{ij} - e_{ij}^\mathrm{v}, \varphi - \beta\varepsilon_\mathrm{v}^\mathrm{v}, A - A^\mathrm{v}\right) = \frac{1}{2}\sigma_m\varepsilon_\mathrm{v}^\mathrm{e} + \frac{1}{2}s_{ij}e_{ij}^\mathrm{e} + \frac{1}{2}P_\mathrm{L}\Delta\varphi^\mathrm{e} + \frac{1}{2}\gamma_\mathrm{SL}\Delta A^\mathrm{e}. \tag{22b}$$

According to Eq. (2), A^e is related to φ^e. The elastic work W_s depends on $\varepsilon_\mathrm{v}^\mathrm{e}$, e_{ij}^e and φ^e for a linear isotropic material and can be written as

$$W_\mathrm{s}\left(\varepsilon_\mathrm{v}^\mathrm{e}, e_{ij}^\mathrm{e}, \varphi^\mathrm{e}\right) = \frac{1}{2}\sigma_m\varepsilon_\mathrm{v}^\mathrm{e} + \frac{1}{2}s_{ij}e_{ij}^\mathrm{e} + \frac{1}{2}P_\mathrm{L}(\varphi^\mathrm{e} - \varphi_0) + \frac{\gamma_\mathrm{SL}}{2r_\mathrm{p}}(\varphi^\mathrm{e} - \varphi_0). \tag{23}$$

Substituting Eqs. (18), (20), (22) and (23) into Eq. (1) gives the state equation for the isothermal and isotropic rock skeleton in the following form (see "Appendix C"):

$$\sigma_m\mathrm{d}\varepsilon_\mathrm{v} + s_{ij}\mathrm{d}e_{ij} + P_\mathrm{C}\mathrm{d}\varphi_C + P_\mathrm{L}\mathrm{d}\varphi_\mathrm{L} + \gamma_\mathrm{SL}\mathrm{d}A - \mathrm{d}F_\mathrm{s} = \left(\sigma_m + \beta P_\mathrm{L} + \frac{\gamma_\mathrm{SL}}{r_\mathrm{p}}\beta - \kappa\varepsilon_v^v\right)\mathrm{d}\varepsilon_\mathrm{v}^\mathrm{v} + \left(s_{ij} - 2\varsigma e_{ij}^\mathrm{v}\right)\mathrm{d}e_{ij}^\mathrm{v} \geq 0. \tag{24}$$

In order to deduce the constitutive equations from Eq. (24), the following dissipation function is defined to express the right-hand side of Eq. (24) as the dissipation part in this inequality:

$$F_\mathrm{D} = \left(\sigma_m + \beta P_\mathrm{L} + \frac{\gamma_\mathrm{SL}}{r_\mathrm{p}}\beta - \kappa\varepsilon_\mathrm{v}^\mathrm{v}\right)\dot{\varepsilon}_\mathrm{v}^\mathrm{v} + \left(s_{ij} - 2\varsigma e_{ij}^\mathrm{v}\right)\dot{e}_{ij}^\mathrm{v}. \tag{25}$$

The partial derivative of F_D with respect to $\dot{\varepsilon}_\mathrm{v}^\mathrm{v}$ and $\dot{e}_{ij}^\mathrm{v}$ are represented, respectively, as

$$\left(\sigma_m + \beta P_\mathrm{L} + \frac{\gamma_\mathrm{SL}}{r_\mathrm{p}}\beta - \kappa\varepsilon_\mathrm{v}^\mathrm{v}\right) = \frac{\partial F_\mathrm{D}}{\partial\dot{\varepsilon}_\mathrm{v}^\mathrm{v}}, \tag{26a}$$

$$\left(s_{ij} - 2\varsigma e_{ij}^\mathrm{v}\right) = \frac{\partial F_\mathrm{D}}{\partial\dot{e}_{ij}^\mathrm{v}}. \tag{26a}$$

Similar to U in Eq. (20), F_D as a function of $\dot{\varepsilon}_\mathrm{v}^\mathrm{v}$ and $\dot{e}_{ij}^\mathrm{v}$ can also be given as

$$F_{\mathrm{D}}\left(\dot{\varepsilon}_{\mathrm{v}}^{\mathrm{v}}, \dot{e}_{ij}^{\mathrm{v}}\right) = \frac{1}{2}\zeta\dot{\varepsilon}_{\mathrm{v}}^{\mathrm{v}2} + \eta\dot{e}_{ij}^{\mathrm{v}2} \geq 0, \tag{27}$$

where ζ and η are the coefficients of the dissipation function which are positive and can be identified as the volumetric viscous coefficient and the shear viscous coefficient, respectively.

Substituting Eq. (27) into Eq. (26), the viscoelastic constitutive equations for isothermal changes and isotropic porous materials with crystallization are expressed as

$$\sigma_m + \beta P_{\mathrm{L}} + \frac{\gamma_{\mathrm{SL}}}{r_{\mathrm{p}}}\beta = \kappa\varepsilon_{\mathrm{v}}^{\mathrm{v}} + \zeta\dot{\varepsilon}_{\mathrm{v}}^{\mathrm{v}}, \tag{28a}$$

$$s_{ij} = 2\varsigma e_{ij}^{\mathrm{v}} + 2\eta\dot{e}_{ij}^{\mathrm{v}}, \tag{28b}$$

where the coefficients κ, ζ, ς and η are to be determined.

4 Determination of the Parameters in the Viscoelasticity Model

To determine the parameters in Eq. (28), we consider a process under constant stress. The strain versus time relationship in Eq. (28) is then first deduced in the form:

$$\varepsilon_{\mathrm{v}}^{\mathrm{v}} = \left(\sigma_m + \beta P_{\mathrm{L}} + \frac{\gamma_{\mathrm{SL}}}{r_{\mathrm{p}}}\beta\right)\frac{1}{\kappa}\left(1 - e^{-\frac{\kappa}{\zeta}t}\right), \tag{29a}$$

$$e_{ij}^{\mathrm{v}} = s_{ij}\frac{1}{2\varsigma}\left(1 - e^{-\frac{2\varsigma}{\eta}t}\right). \tag{29b}$$

The parameters in Eq. (28) can be determined according to the empirical formulae and creep test results at every deviator stress level in Sect. 2.3. For example, for the first deviator stress level of the creep tests in Sect. 2.3, the sandstone was under constant stress: $\sigma_3 = 5$ MPa and $\sigma_1 - \sigma_3 = 10$ MPa. The process reached a steady state where the strain rate was small enough for it to be assumed that $\dot{\varepsilon}_{\mathrm{v}}^{\mathrm{v}} = \dot{e}_{ij}^{\mathrm{v}} = 0$ in Eq. (28). As the crystallization is in the quasi-static equilibrium state which satisfies phase equilibrium, the interfacial energy γ_{SL} is constant during the small deformation. In the creep test, σ_m and s_{ij} are given; β is from 1 to φ_0; P_{L} can be calculated by using the Skempton coefficients (Table 2) and $\sigma_m = (\sigma_1 + \sigma_2 + \sigma_3)/3$. The rest of the parameters are determined by using the methods in the following sub-sections.

4.1 Determination of $\frac{\gamma_{\mathrm{SL}}}{r_{\mathrm{p}}}\beta$

For a NaCl solution with a mass fraction between 0.14 and 25.96 % and temperature between 0 and 30 °C, an expression for the surface tension of the solution can be obtained from the literature (Seawater desalination manual 1974) in the form,

$$\gamma_{\mathrm{L}} = 7.549 \times 10^{-2} + 3.670 \times 10^{-2}c - 1.485 \times 10^{-4}t. \tag{30}$$

According to Young's equation (Adamson 1990):

$$\gamma_{\mathrm{SL}} = \gamma_{\mathrm{S}} - \gamma_{\mathrm{L}}\cos\psi, \tag{31}$$

where ψ is the contact angle between the saturated NaCl solution and sandstone (Table 3).

Since β is from 1 to φ_0, the range of $\frac{\gamma_{\mathrm{SL}}}{r_{\mathrm{p}}}\beta$ in Eq. (29) for the sandstone specimen without in-pore NaCl crystals can be deduced to be 0.01883 MPa $\leq \frac{\gamma_{\mathrm{SL}}}{r_{\mathrm{p}}}\beta \leq$ 0.08505 MPa.

For the sandstone with in-pore NaCl crystal, the experimental formula Eq. (30) is not applicable (Table 4). Substituting Eqs. (4), (7), and (8) into Eq. (9) gives

$$\frac{\gamma_{\mathrm{SL}}}{r_{\mathrm{p}}} = P_{\mathrm{L}} + \frac{RT}{2v_{\mathrm{C}}}\ln\left(\frac{a}{a_0}\right) - P_S.$$

The corresponding range of $\frac{\gamma_{\mathrm{SL}}}{r_{\mathrm{p}}}\beta$ for samples with in-pore NaCl crystals is calculated as 0.3037 MPa $\leq \frac{\gamma_{\mathrm{SL}}}{r_{\mathrm{p}}}\beta \leq$ 1.3710 MPa.

Table 3 Parameters to determine $\frac{\gamma_{\mathrm{SL}}}{r_{\mathrm{p}}}\beta$ for sandstone without in-pore NaCl crystals

Parameters	Surface energy of saturated NaCl solution, γ_{L} (mJ/m^2)	Surface energy of rock, γ_{S} (mJ/m^2)	Contact angle, ψ (°)	Liquid–solid interfacial energy, γ_{SL} (mJ/m^2)	Porosity, φ_0	Mean pore radius, r_{p} (μm)
Value	81.52	208.76	57.3	164.68	22.15 %	1.93639
Method	Eq. (30)	Tracer liquid and contact angle meter	Contact angle meter	Eq. (31)	Saturation and caliper techniques	Eq. (3)

Table 4 Parameters to determine $\frac{\gamma_{\mathrm{SL}}}{r_{\mathrm{p}}}\beta$ for sandstone with in-pore NaCl crystals

Parameters	Pore liquid pressure, P_{L} (MPa)	Total normal stress on pore surface, P_{S} (MPa)	Activity of solution, a (mol/L)	Equilibrium activity of solution, a_0 (mol/L)	Molar volume of NaCl crystal, v_{C} (cm^3/mol)
Value	1.7233	8.3333	6.1149	5.2001	24.55
Method	"Appendix D"	"Appendix D"	Cohen (1988)	Cohen (1988)	(Scherer 1999)

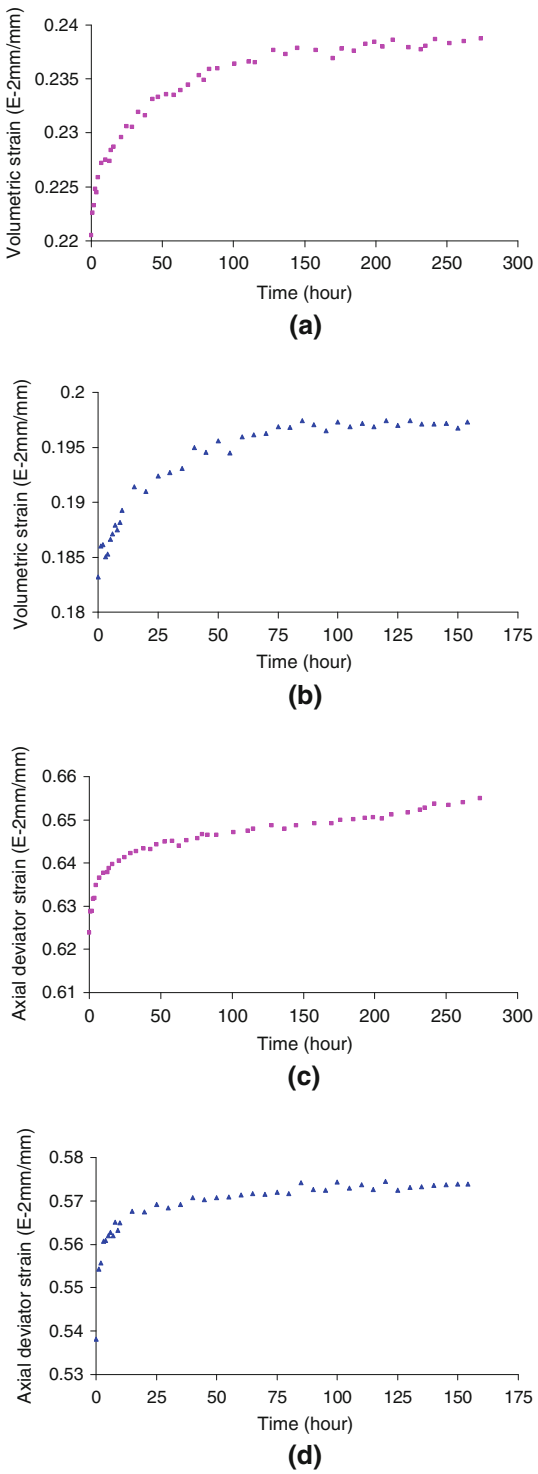

Fig. 12 Volumetric strain versus time for the first level creep tests showing **a** sandstone without in-pore NaCl crystals, and **b** sandstone with in-pore NaCl crystals. The axial deviator strain versus time plots for the first level creep test are shown for **c** sandstone without in-pore NaCl crystals, and **d** sandstone with in-pore NaCl crystals (confining pressure $\sigma_3 = 5$ MPa; deviated stress $\sigma_1 - \sigma_3 = 10$ MPa)

4.2 Determination of the Model Coefficients

The relationships among the viscosity model parameters, bulk modulus, and shear modulus are obtained from Coussy (2004) as:

$$\frac{1}{K_0} + \frac{1}{\kappa} = \frac{1}{K_\infty}; \quad \frac{1}{G_0} + \frac{1}{\varsigma} = \frac{1}{G_\infty}. \tag{32}$$

For the first deviator stress level used in the creep tests, the total strain is divided into volumetric strain and deviator strain. To determine the coefficients, plots of the volumetric strain and axial deviator strain (i.e., $\varepsilon_1 = \varepsilon_1 - \varepsilon_v/3$) versus time for the sandstones with and without in-pore crystals are obtained as shown in Fig. 12. The corresponding coefficients derived from the creep test results are summarized in Table 5.

According to the initial conditions $\dot{\varepsilon}_v^v(t=0) = \left(\sigma_m + \beta P_L + \frac{\gamma_{SL}}{r_p}\beta\right)\frac{1}{\zeta}$ and $\dot{e}_1^v(t=0) = s_1\frac{1}{\eta}$ from Eq. (29), and so the coefficients ζ and η can be calculated. Using the lower and upper bounds of β, the lower and upper bounds of the dissipation function coefficient ζ for the sandstone without in-pore NaCl crystals are 1.5755×10^6 and 2.0968×10^6 MPa h, respectively. The two bounds for the sandstone with in-pore NaCl crystals are 1.5775×10^6 and 1.8930×10^6 MPa h, respectively. The dissipation function coefficients η for the saturated sandstones and the oversaturated sandstones are 7.95391×10^5 and 2.15391×10^5 MPa h, respectively.

Model curves (Fig. 13) of the constitutive equation Eq. (29) are created to compare with the visco-volumetric strain versus time and axial visco-deviator strain versus time data. The test result curves in Fig. 13 are obtained from Fig. 12 by removing the instantaneous strain.

It can be seen from Fig. 13 that the established model is quite acceptable. Also, the model results for the visco-volumetric strain versus time of both sandstones are better than those for the axial visco-deviator strain versus time. The reason for this may be related to the hypothesis that the material is isotropic. In reality, property parameters such as the Biot tensor are anisotropic and make some contribution to s_{ij}. Therefore, anisotropy should be taken into account in further studies.

5 Discussion

The viscoelastic poromechanical model developed in this paper is intended to describe the long-term mechanical behavior of sandstone with NaCl crystallized in its pores

Table 5 Bulk and shear moduli at the onset of creep and steady state creep for sandstone with and without in-pore NaCl crystals

	K_0 (MPa)	K_∞ (MPa)	G_0 (MPa)	G_∞ (MPa)	κ (MPa)	ς (MPa)
Sandstone without in-pore NaCl crystal	3,777.58	3,489.07	534.41	508.89	45,682.99	10,658.47
Sandstone with in-pore NaCl crystal	4,549.47	4,360.53	619.40	580.84	104,998.76	9,331.36

based on thermochemistry. The model is restricted to isothermal changes and isotropic materials. If the effect of NaCl crystallization and interfacial energy in Eq. (1) is ignored, the viscoelastic poromechanical model for an isothermal process and linear isotropic material in Eqs. (18) and (28) reduce to Eqs. (4.62) under isothermal conditions and (9.14) in Coussy (2004), i.e.,

$$\mathrm{d}\sigma_m = K\mathrm{d}\varepsilon_{\mathrm{v}}^{\mathrm{e}} - b\mathrm{d}P,$$

$$\mathrm{d}s_{ij} = 2G\mathrm{d}e_{ij}^{\mathrm{e}},$$

$$\sigma_m + \beta P_{\mathrm{L}} = \kappa\varepsilon_{\mathrm{v}}^{\mathrm{v}} + \zeta\dot{\varepsilon}_{\mathrm{v}}^{\mathrm{v}},$$

$$s_{ij} = 2\varsigma e_{ij}^{\mathrm{v}} + 2\eta\dot{e}_{ij}^{\mathrm{v}}.$$

Compared with the above model, Eq. (18) and (28) can quantify the impact of crystallization on the mechanical properties in terms of the pores' geometric sizes and the interfacial energy between the pore fluid and rock solid. When crystallization occurs in porous material, the crystallization pressure driven by supersaturation can exert itself on the pore surface. These influences are embodied in the solid–liquid interfacial energy $\frac{\gamma_{\mathrm{SL}}}{r_{\mathrm{p}}} = P_{\mathrm{L}} + \frac{RT}{2v_{\mathrm{C}}}\ln\left(\frac{C}{C_0}\right) - P_{\mathrm{S}}$. Therefore, to describe the influence of crystals on the poromechanical properties, it is reasonable to add in the interfacial energy factor to the constitutive relations.

6 Conclusions

The influence of NaCl crystallization on the long-term mechanical behavior of sandstone has been investigated using laboratory isothermal tests and theoretical analysis. A series of laboratory isothermal tests including uniaxial and triaxial compressive tests, creep tests, and poromechanical tests on sandstone with and without in-pore NaCl crystals have been conducted. The test results indicate that NaCl crystallization in pores enhances the compressive strength and bulk modulus under a given confining pressure and reduces creep (for example, the difference between initial and final value of the axial strain during each creep level and the time taken to reach stable creep). In addition, it makes the pore liquid pressure in the sandstone less sensitive to changes in hydrostatic stress under undrained conditions. These test results are important for estimation of the reservoir's stability during carbon dioxide sequestration in saline aquifers, especially in the dry-out region closest to the wellbore.

To estimate the effect of in-pore crystallization on the long-term mechanical behavior of the reservoir, a poro-viscoelastic model for isothermal changes and isotropic porous materials with crystals in the pores is proposed in this paper. Based on an assumed geometrical model for the crystal-in-pore framework, a mechanical model is set up by quantifying the influence of the interfacial energies and pore size distribution on the effective stress in terms of crystal pressure during deformation. The pore stress distribution tensor and the interfacial energy are used as the link in a chemical–mechanical coupling of the porous material with the crystallization in the pores. These mechanical constitutive relationships are established under the precondition of a quasi-static equilibrium state in the crystal growth. Moreover, the maximal crystal pressure on the pore surface is used for the quasi-static equilibrium state on the basis of crystal growth theory and thermodynamics to maximize the impact of crystallization. With the relationship between pore volume and pore surface area based on the geometrical model, the solid–liquid interfacial energy on the pore surface area can be expediently included into the state equation. The viscoelastic constitutive equations for isothermal changes and isotropic porous materials with crystallization were thus established. This model reduces to Eqs. (4.62) under isothermal conditions and (9.14) in Coussy (2004) by ignoring the effect of NaCl crystallization and interfacial energy.

By comparing the output of the model and test results, it was shown that the poro-viscoelasitic model is acceptable. The agreement between the output from the model of the axial visco-deviator strain variation versus time for the sandstone with and without crystals and the test results is a little bit weaker than the model output for the visco-volumetric strain versus time. This is due to the hypothesis that the material is isotropic. Thus, the effects of property parameters (such as the Biot tensor) on the deviator strain, is ignored. Therefore, anisotropy in these properties should be taken into account in future studies. Furthermore, the underground temperature gradient affects the porous rock dilation and the supersaturation of the pore fluid. As the result of this, anisothermal evolution should also be considered in future research.

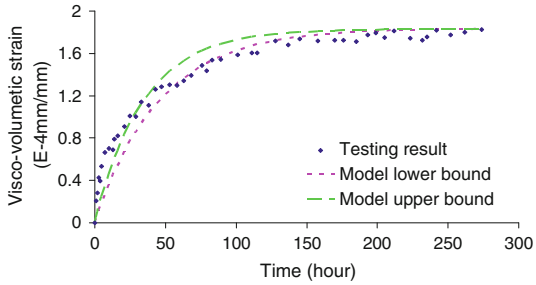

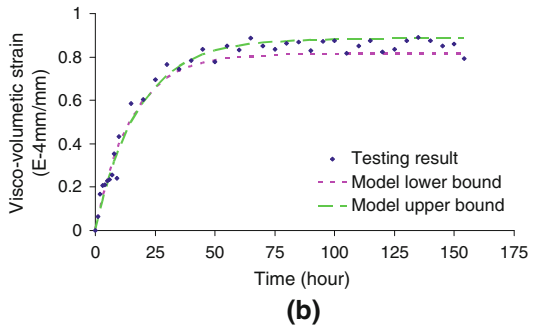

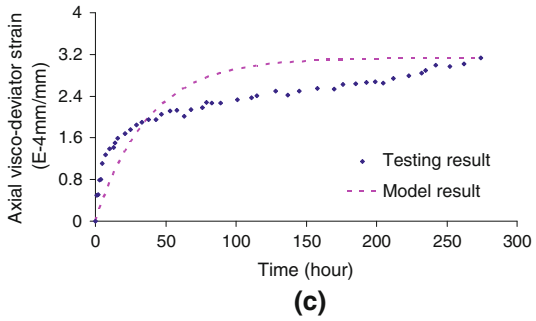

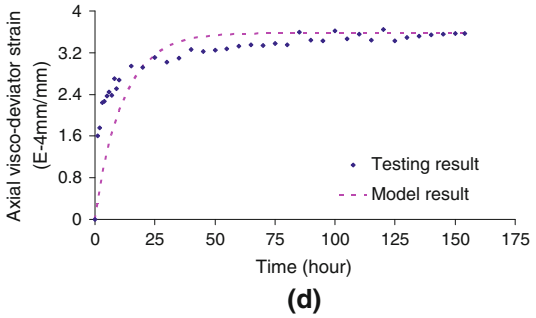

Fig. 13 Visco-volumetric strain versus time and lower and upper bound model curves of **a** sandstone without in-pore NaCl crystals, and **b** sandstone with in-pore NaCl crystals. Also shown are the axial visco-deviator strain versus time and model curves of **c** sandstone without in-pore NaCl crystals, and **d** sandstone with in-pore NaCl crystals (confining pressure $\sigma_3 = 5$ MPa; deviator stress $\sigma_1 - \sigma_3 = 10$ MPa)

The pore-size distribution is calculated from capillary entry pressure and cumulative intrusion volume measurements via mercury intrusion porosimetry experiments. During in-pore crystallization, salt crystals grow preferentially in the largest pores. When a coarse pore is filled with crystals, crystallization continues in the smaller pores connected to it (Pruess and Spycher 2007). So, the calculation method used for the pore radius in the geometrical model within the crystal-in-pore framework could be further improved in subsequent studies by considering the pore-size distribution and the degree of crystallization at the same time.

Acknowledgments This work received financial support from the National Natural Science Foundation of China (Grant No. 11232024). Professors Yossef Hatzor and Einat Haronov gave helpful suggestions to improve this manuscript. They are all gratefully acknowledged.

Appendices

Appendix A: The Solution Process for Eq. (16)

According to Maxwell's symmetry relations, the partial differential of the variables in Eq. (14) are

$$\frac{\partial \sigma_{ij}}{\partial P_{\mathrm{J}}} = -\frac{\partial \varphi_{\mathrm{J}}^{\mathrm{e}}}{\partial \varepsilon_{ij}^{\mathrm{e}}};\ \frac{\partial \varphi_{\mathrm{J}}}{\partial T} = \frac{\partial S_{\mathrm{s}}}{\partial P_{\mathrm{J}}};\ \frac{\partial \varphi_{\mathrm{J}}}{\partial A^{\mathrm{e}}} = -\frac{\partial \gamma_{\mathrm{SL}}}{\partial P_{\mathrm{J}}};$$
$$\frac{\partial \sigma_{ij}}{\partial T} = -\frac{\partial S_{\mathrm{s}}}{\partial \varepsilon_{ij}^{\mathrm{e}}};\ \frac{\partial \sigma_{ij}}{\partial A^{\mathrm{e}}} = \frac{\partial \gamma_{\mathrm{SL}}}{\partial \varepsilon_{ij}^{\mathrm{e}}};\ \frac{\partial S_{\mathrm{s}}}{\partial A^{\mathrm{e}}} = -\frac{\partial \gamma_{\mathrm{SL}}}{\partial T}.$$

From Eqs. (9) and (12), the partial derivatives of P_S with respect to γ_{SL} and σ_{ij} can be written as:

$$\frac{\partial P_{\mathrm{S}}}{\partial \gamma_{\mathrm{SL}}} = -\frac{1}{r_{\mathrm{p}}};\ \frac{\partial P_{\mathrm{S}}}{\partial \sigma_{ij}} = R_{ij}.$$

Other partial derivative can be expressed as follows:

$$\frac{\partial \sigma_{ij}}{\partial A^{\mathrm{e}}} = \frac{\partial \gamma_{\mathrm{SL}}}{\partial \varepsilon_{ij}^{\mathrm{e}}} = \frac{\partial \gamma_{\mathrm{SL}}}{\partial P_{\mathrm{S}}}\frac{\partial P_{\mathrm{S}}}{\partial \sigma_{kl}}\frac{\partial \sigma_{kl}}{\partial \varepsilon_{ij}^{\mathrm{e}}} = -r_{\mathrm{p}} R_{kl} C_{ijkl},$$

$$\frac{\partial \sigma_{ij}}{\partial P_{\mathrm{J}}} = -\frac{\partial \varphi_{\mathrm{J}}^{\mathrm{e}}}{\partial \varepsilon_{ij}^{\mathrm{e}}} = -b_{ij}^{\mathrm{J}},$$

$$\frac{\partial \varphi_{\mathrm{J}}^{\mathrm{e}}}{\partial T} = \frac{\partial S_{\mathrm{s}}}{\partial P_{\mathrm{J}}} = -3\alpha_{\varphi}^{\mathrm{J}},$$

$$\frac{\partial \sigma_{ij}}{\partial T} = -\frac{\partial S_{\mathrm{s}}}{\partial \varepsilon_{ij}^{\mathrm{e}}} = \frac{\partial \sigma_{ij}}{\partial \varepsilon_{kl}^{\mathrm{e}}}\frac{\partial \varepsilon_{kl}^{\mathrm{e}}}{\partial T} = -C_{ijkl}\alpha_{kl},$$

$$\frac{\partial S_{\mathrm{s}}}{\partial A^{\mathrm{e}}} = -\frac{\partial \gamma_{\mathrm{SL}}}{\partial T} = -\frac{\partial \gamma_{\mathrm{SL}}}{\partial \varepsilon_{ij}^{\mathrm{e}}}\frac{\partial \varepsilon_{ij}^{\mathrm{e}}}{\partial T} = -r_{\mathrm{p}} R_{kl} C_{ijkl}\alpha_{ij},$$

$$\frac{\partial \gamma_{\mathrm{SL}}}{\partial A^{\mathrm{e}}} = \frac{\partial \gamma_{\mathrm{SL}}}{\partial \sigma_{ij}}\frac{\partial \sigma_{ij}}{\partial A^{\mathrm{e}}} = \frac{\partial \gamma_{\mathrm{SL}}}{\partial P_{\mathrm{S}}}\frac{\partial P_{\mathrm{S}}}{\partial \sigma_{ij}}\frac{\partial \sigma_{ij}}{\partial A^{\mathrm{e}}} = r_{\mathrm{p}}^2 R_{ij} R_{kl} C_{ijkl},$$

$$\frac{\partial \varphi^{\mathrm{e}}}{\partial A^{\mathrm{e}}} = \frac{\partial \varphi_{\mathrm{C}}^{\mathrm{e}}}{\partial A^{\mathrm{e}}} + \frac{\partial \varphi_{\mathrm{L}}^{\mathrm{e}}}{\partial A^{\mathrm{e}}} = -\left(\frac{\partial \gamma_{\mathrm{SL}}}{\partial P_{\mathrm{C}}} + \frac{\partial \gamma_{\mathrm{SL}}}{\partial P_{\mathrm{L}}}\right) = \frac{r_{\mathrm{p}}}{2}.$$

Appendix B: Main Formulas used to Deduce Eq. (18)

The pore stress distribution factor R_{ij} is written as:

$$R_{ij}=\frac{\int_0^{2\pi} Q_j Q_i \mathrm{d}\alpha_1}{2\pi}=\frac{1}{2\pi}\int_0^{2\pi}\begin{pmatrix} l^2 & lm & nl \\ ml & m^2 & mn \\ nl & mn & n^2 \end{pmatrix}$$

$$\mathrm{d}\alpha_1=\begin{pmatrix} r_{11} & r_{12} & r_{13} \\ r_{21} & r_{22} & r_{23} \\ r_{31} & r_{32} & r_{33} \end{pmatrix},$$

where

$$l=\cos\theta_1=\cos\alpha_1\cdot\sin\phi_1,\ m=\cos\theta_2=\cos\alpha_2\cdot\sin\phi_2,$$
$$n=\cos\theta_3=\cos\alpha_3\cdot\sin\phi_3,$$

$$r_{11}+r_{22}+r_{33}=\frac{\int_0^{2\pi}(l^2+m^2+n^2)\mathrm{d}\alpha_1}{2\pi}=\frac{\int_0^{2\pi}(\cos^2\theta_1+\cos^2\theta_2+\cos^2\theta_3)\mathrm{d}\alpha_1}{2\pi}=1.$$

For an isotropic linear poroelastic material, the elastic stiffness modulus is written as:

$$C_{ijkl}=\begin{bmatrix} \lambda+2G & \lambda & \lambda & 0 & 0 & 0 \\ \lambda & \lambda+2G & \lambda & 0 & 0 & 0 \\ \lambda & \lambda & \lambda+2G & 0 & 0 & 0 \\ 0 & 0 & 0 & G & 0 & 0 \\ 0 & 0 & 0 & 0 & G & 0 \\ 0 & 0 & 0 & 0 & 0 & G \end{bmatrix}.$$

Accordingly,

$$C_{ijkl}R_{kl}=\begin{bmatrix} (r_{11}+r_{22}+r_{33})\lambda+2r_{11}G & 2r_{12}G & 2r_{13}G \\ 2r_{12}G & (r_{11}+r_{22}+r_{33})\lambda+2r_{22}G & 2r_{23}G \\ 2r_{13}G & 2r_{23}G & (r_{11}+r_{22}+r_{33})\lambda+2r_{33}G \end{bmatrix}$$
$$=\left(\lambda+\frac{2}{3}G\right)\delta_{ij}+\begin{bmatrix} \frac{2}{3}(2r_{11}-r_{22}-r_{33})G & 2r_{12}G & 2r_{13}G \\ 2r_{12}G & \frac{2}{3}(2r_{22}-r_{11}-r_{33})G & 2r_{23}G \\ 2r_{13}G & 2r_{23}G & \frac{2}{3}(2r_{33}-r_{22}-r_{11})G \end{bmatrix}$$
$$=K\delta_{ij}+\chi_{ij},$$

where $K=\lambda+\frac{2}{3}G$, and

$$\chi_{ij}=\begin{bmatrix} \frac{2}{3}(2r_{11}-r_{22}-r_{33})G & 2r_{12}G & 2r_{13}G \\ 2r_{12}G & \frac{2}{3}(2r_{22}-r_{11}-r_{33})G & 2r_{23}G \\ 2r_{13}G & 2r_{23}G & \frac{2}{3}(2r_{33}-r_{22}-r_{11})G \end{bmatrix}.$$

Therefore, $R_{ij}C_{ijkl}R_{kl}=K+R_{ij}\chi_{ij}=K+\chi$. Here, χ is scalar and $\chi=R_{ij}\chi_{ij}$.

For an isotropic linear poroelastic material, the crystal/liquid Biot tangent tensor is isotropic and $b_{ij}^{\mathrm{J}}=b^{\mathrm{J}}\delta_{ij}$. Because $\sigma_{ij}=\sigma_m\delta_{ij}+s_{ij}$, $\varepsilon_{ij}=\frac{\varepsilon_{\mathrm{v}}}{3}\delta_{ij}+e_{ij}$, so

$$C_{ijkl}R_{kl}\varepsilon_{ij}^{\mathrm{e}}=C_{ijkl}R_{kl}\left(\frac{\varepsilon_{\mathrm{v}}^{\mathrm{e}}}{3}\delta_{ij}+e_{ij}^{\mathrm{e}}\right)=K\varepsilon_{\mathrm{v}}^{\mathrm{e}}+\chi_{ij}e_{ij}^{\mathrm{e}}.$$

Appendix C: The Solution Process for Eq. (24)

The elastic work W_{s} and viscous deformation energy U are

$$\begin{aligned}
W_{\mathrm{s}}\left(\varepsilon_{\mathrm{v}}^{\mathrm{e}},e_{ij}^{\mathrm{e}},\varphi^{\mathrm{e}}\right)&=W_{\mathrm{s}}\left(\varepsilon_{\mathrm{v}}-\varepsilon_{\mathrm{v}}^{\mathrm{v}},e_{ij}-e_{ij}^{\mathrm{v}},\varphi-\beta\varepsilon_{\mathrm{v}}^{\mathrm{v}}\right)\\
&=\frac{1}{2}\sigma_{\mathrm{m}}\varepsilon_{\mathrm{v}}+\frac{1}{2}s_{ij}e_{ij}+\frac{1}{2}P\cdot\Delta\varphi+\frac{\gamma_{\mathrm{SL}}}{2r_{\mathrm{p}}}\cdot\Delta\varphi\\
&=\frac{1}{2}\varepsilon_{\mathrm{v}}^{\mathrm{e}}\left[K\varepsilon_{\mathrm{v}}^{\mathrm{e}}-\left(b^{\mathrm{C}}+b^{\mathrm{L}}\right)P_{\mathrm{L}}-K(\varphi^{\mathrm{e}}-\varphi_0)\right]\\
&\quad+\left[Ge_{ij}^{\mathrm{e}}-\frac{\chi_{ij}}{2}(\varphi^{\mathrm{e}}-\varphi_0)\right]e_{ij}^{\mathrm{e}}+\frac{1}{2}P_{\mathrm{L}}\left(\varphi_{\mathrm{L}}^{\mathrm{e}}-\varphi_{L0}\right)\\
&\quad+\frac{1}{2}\left(P_{\mathrm{L}}+\frac{2\gamma_{CL}}{r_{\mathrm{p}}-\delta}\right)\left(\varphi_{\mathrm{C}}^{\mathrm{e}}-\varphi_{C0}\right)\\
&\quad+\frac{1}{2}\left[\left(-K\varepsilon_{\mathrm{v}}^{\mathrm{e}}-\chi_{ij}e_{ij}^{\mathrm{e}}\right)-\frac{P_{\mathrm{L}}}{2}+(K+\chi)(\varphi^{\mathrm{e}}-\varphi_0)\right](\varphi^{\mathrm{e}}-\varphi_0)\\
&=\frac{1}{2}K\left(\varepsilon_{\mathrm{v}}-\varepsilon_{\mathrm{v}}^{\mathrm{v}}\right)^2-K(\varphi^{\mathrm{e}}-\varphi_0)\left(\varepsilon_{\mathrm{v}}-\varepsilon_{\mathrm{v}}^{\mathrm{v}}\right)\\
&\quad-\frac{P_{\mathrm{L}}}{2}\left[\left(\varepsilon_{\mathrm{v}}-\varepsilon_{\mathrm{v}}^{\mathrm{v}}\right)\left(b^{\mathrm{C}}+b^{\mathrm{L}}\right)-\frac{1}{2}(\varphi^{\mathrm{e}}-\varphi_0)\right]+G\left(e_{ij}-e_{ij}^{\mathrm{v}}\right)^2\\
&\quad-\chi_{ij}\left(e_{ij}-e_{ij}^{\mathrm{v}}\right)(\varphi^{\mathrm{e}}-\varphi_0)+\frac{1}{2}(K+\chi)(\varphi^{\mathrm{e}}-\varphi_0)^2\\
&\quad+\frac{\gamma_{\mathrm{CL}}}{r_{\mathrm{p}}-\delta}\left(\varphi_{\mathrm{C}}^{\mathrm{e}}-\varphi_{C0}\right)\\
&=\frac{1}{2}K\left(\varepsilon_{\mathrm{v}}-\varepsilon_{\mathrm{v}}^{\mathrm{v}}\right)^2+\frac{1}{2\left[\frac{1}{N_{LL}}+\frac{2}{N_{\mathrm{LC}}}+\frac{1}{N_{\mathrm{CC}}}\right]}\\
&\quad\times\left[\frac{1}{2}(\varphi^{\mathrm{e}}-\varphi_0)-\left(\varepsilon_{\mathrm{v}}-\varepsilon_{\mathrm{v}}^{\mathrm{v}}\right)\left(b^{\mathrm{C}}+b^{\mathrm{L}}\right)\right]^2+G\left(e_{ij}-e_{ij}^{\mathrm{v}}\right)^2\\
&\quad-K(\varphi^{\mathrm{e}}-\varphi_0)\left(\varepsilon_{\mathrm{v}}-\varepsilon_{\mathrm{v}}^{\mathrm{v}}\right)-\chi_{ij}\left(e_{ij}-e_{ij}^{\mathrm{v}}\right)(\varphi^{\mathrm{e}}-\varphi_0)\\
&\quad+\frac{1}{2}(K+\chi)(\varphi^{\mathrm{e}}-\varphi_0)^2+\frac{\gamma_{\mathrm{CL}}}{r_p-\delta}\left(\varphi_C^{\mathrm{e}}-\varphi_{C0}\right).
\end{aligned}$$

$$U(\varepsilon_{\mathrm{v}}^{\mathrm{v}},e_{ij}^{\mathrm{v}})=\frac{1}{2}k\varepsilon_{\mathrm{v}}^{\mathrm{v}^2}+\zeta e_{ij}^{\mathrm{v}^2}$$

So, we get the incremental form of free energy, F_{s}:

$$\begin{aligned}
\mathrm{d}F_{\mathrm{s}}&=K\left(\varepsilon_{\mathrm{v}}-\varepsilon_{\mathrm{v}}^{\mathrm{v}}\right)\left(\mathrm{d}\varepsilon_{\mathrm{v}}-\mathrm{d}\varepsilon_{\mathrm{v}}^{\mathrm{v}}\right)-K\left(\varepsilon_{\mathrm{v}}-\varepsilon_{\mathrm{v}}^{\mathrm{v}}\right)\left(\mathrm{d}\varphi-\beta\mathrm{d}\varepsilon_{\mathrm{v}}^{\mathrm{v}}\right)\\
&\quad-K\left(\mathrm{d}\varepsilon_{\mathrm{v}}-\mathrm{d}\varepsilon_{\mathrm{v}}^{\mathrm{v}}\right)\left(\varphi-\beta\varepsilon_{\mathrm{v}}^{\mathrm{v}}-\varphi_0\right)+\frac{1}{\left[\frac{1}{N_{\mathrm{LL}}}+\frac{2}{N_{\mathrm{LC}}}+\frac{1}{N_{\mathrm{CC}}}\right]}\\
&\quad\times\left[\frac{1}{2}(\varphi^{\mathrm{e}}-\varphi_0)-\left(\varepsilon_{\mathrm{v}}-\varepsilon_{\mathrm{v}}^{\mathrm{v}}\right)\left(b^{\mathrm{C}}+b^{\mathrm{L}}\right)\right]\\
&\quad\times\left[\frac{1}{2}\left(\mathrm{d}\varphi-\beta\mathrm{d}\varepsilon_{\mathrm{v}}^{\mathrm{v}}\right)-\left(b^{\mathrm{C}}+b^{\mathrm{L}}\right)\left(\mathrm{d}\varepsilon_{\mathrm{v}}-\mathrm{d}\varepsilon_{\mathrm{v}}^{\mathrm{v}}\right)\right]
\end{aligned}$$

$$
\begin{aligned}
&-\chi_{ij}\left(\mathrm{d}\varepsilon_{\mathrm{v}}-\mathrm{d}\varepsilon_{\mathrm{v}}^{\mathrm{v}}\right)\left(\varphi-\beta\varepsilon_{\mathrm{v}}^{\mathrm{v}}-\varphi_0\right)-\chi_{ij}\left(\varepsilon_{\mathrm{v}}-\varepsilon_{\mathrm{v}}^{\mathrm{v}}\right)\left(\mathrm{d}\varphi-\beta\mathrm{d}\varepsilon_{\mathrm{v}}^{\mathrm{v}}\right)\\
&+(K+\chi)\left(\varphi-\beta\varepsilon_{\mathrm{v}}^{\mathrm{v}}-\varphi_0\right)\left(\mathrm{d}\varphi-\beta\mathrm{d}\varepsilon_{\mathrm{v}}^{\mathrm{v}}\right)\\
&+2G\left(e_{ij}-e_{ij}^{\mathrm{v}}\right)\left(\mathrm{d}e_{ij}-\mathrm{d}e_{ij}^{\mathrm{v}}\right)+\kappa\varepsilon_{\mathrm{v}}^{\mathrm{v}}\mathrm{d}\varepsilon_{\mathrm{v}}^{\mathrm{v}}+2\varsigma e_{ij}^{\mathrm{v}}\mathrm{d}e_{ij}^{\mathrm{v}}\\
&+\frac{\gamma_{\mathrm{CL}}}{r_{\mathrm{p}}-\delta}\left(\mathrm{d}\varphi_{\mathrm{C}}-\mathrm{d}\varphi_{\mathrm{C}}^{\mathrm{v}}\right)\\
=&K\left(\varepsilon_{\mathrm{v}}-\varepsilon_{\mathrm{v}}^{\mathrm{v}}\right)\left(\mathrm{d}\varepsilon_{\mathrm{v}}-\mathrm{d}\varepsilon_{\mathrm{v}}^{\mathrm{v}}\right)-K\left(\varepsilon_{\mathrm{v}}-\varepsilon_{\mathrm{v}}^{\mathrm{v}}\right)\left(\mathrm{d}\varphi-\beta\mathrm{d}\varepsilon_{\mathrm{v}}^{\mathrm{v}}\right)\\
&-K\left(\mathrm{d}\varepsilon_{\mathrm{v}}-\mathrm{d}\varepsilon_{\mathrm{v}}^{\mathrm{v}}\right)\left(\varphi-\beta\varepsilon_{\mathrm{v}}^{\mathrm{v}}-\varphi_0\right)\\
&+P_{\mathrm{L}}\left[\frac{1}{2}\left(\mathrm{d}\varphi-\beta\mathrm{d}\varepsilon_{\mathrm{v}}^{\mathrm{v}}\right)-\left(b^{\mathrm{C}}+b^{\mathrm{L}}\right)\left(\mathrm{d}\varepsilon_{\mathrm{v}}-\mathrm{d}\varepsilon_{\mathrm{v}}^{\mathrm{v}}\right)\right]\\
&-\chi_{ij}\left(\mathrm{d}e_{ij}-\mathrm{d}e_{ij}^{\mathrm{v}}\right)\left(\varphi-\beta\varepsilon_{\mathrm{v}}^{\mathrm{v}}-\varphi_0\right)\\
&-\chi_{ij}\left(e_{ij}-e_{ij}^{\mathrm{v}}\right)\left(\mathrm{d}\varphi-\beta\mathrm{d}\varepsilon_{\mathrm{v}}^{\mathrm{v}}\right)\\
&+(K+\chi)\left(\varphi-\beta\varepsilon_{\mathrm{v}}^{\mathrm{v}}-\varphi_0\right)\left(\mathrm{d}\varphi-\beta\mathrm{d}\varepsilon_{\mathrm{v}}^{\mathrm{v}}\right)\\
&+2G\left(e_{ij}-e_{ij}^{\mathrm{v}}\right)\left(\mathrm{d}e_{ij}-\mathrm{d}e_{ij}^{\mathrm{v}}\right)+\kappa\varepsilon_{\mathrm{v}}^{\mathrm{v}}\mathrm{d}\varepsilon_{\mathrm{v}}^{\mathrm{v}}+2\varsigma e_{ij}^{\mathrm{v}}\mathrm{d}e_{ij}^{\mathrm{v}}\\
&+\frac{\gamma_{\mathrm{CL}}}{r_{\mathrm{p}}-\delta}\left(\mathrm{d}\varphi_{\mathrm{C}}-\mathrm{d}\varphi_{\mathrm{C}}^{\mathrm{v}}\right).
\end{aligned}
$$

Then, substitute the above relationship into Eq. (1) to give

$$
\begin{aligned}
&\sigma_m\mathrm{d}\varepsilon_{\mathrm{v}}+s_{ij}\mathrm{d}e_{ij}+P_{\mathrm{C}}\mathrm{d}\varphi_{\mathrm{C}}+P_{\mathrm{L}}\mathrm{d}\varphi_{\mathrm{L}}+\gamma_{\mathrm{SL}}\mathrm{d}A-\mathrm{d}F_{\mathrm{s}}\\
&=\left[K\left(\varepsilon_{\mathrm{v}}-\varepsilon_{\mathrm{v}}^{\mathrm{v}}\right)-\left(b^{\mathrm{C}}+b^{\mathrm{L}}\right)P_{\mathrm{L}}-K\left(\varphi-\beta\varepsilon_{\mathrm{v}}^{\mathrm{v}}-\varphi_0\right)\right]\mathrm{d}\varepsilon_{\mathrm{v}}\\
&\quad+\left[2G\left(e_{ij}-e_{ij}^{\mathrm{v}}\right)-\chi_{ij}\left(\varphi-\beta\varepsilon_{\mathrm{v}}^{\mathrm{v}}-\varphi_0\right)\right]\mathrm{d}e_{ij}\\
&\quad+P_{\mathrm{L}}\mathrm{d}\varphi+\frac{2\gamma_{\mathrm{CL}}}{r_P-\delta}\mathrm{d}\varphi_{\mathrm{C}}+\left[-K\left(\varepsilon_{\mathrm{v}}-\varepsilon_{\mathrm{v}}^{\mathrm{v}}\right)-\chi_{ij}\left(e_{ij}-e_{ij}^{\mathrm{v}}\right)\right.\\
&\quad\left.-\frac{P_L}{2}+(K+\chi)\left(\varphi-\beta\varepsilon_{\mathrm{v}}^{\mathrm{v}}-\varphi_0\right)\right]\mathrm{d}\varphi-\mathrm{d}F_{\mathrm{s}}\\
&=K\left(\varepsilon_{\mathrm{v}}-\varepsilon_{\mathrm{v}}^{\mathrm{v}}\right)\mathrm{d}\varepsilon_{\mathrm{v}}^{\mathrm{v}}-K\beta\left(\varepsilon_{\mathrm{v}}-\varepsilon_{\mathrm{v}}^{\mathrm{v}}\right)\mathrm{d}\varepsilon_{\mathrm{v}}^{\mathrm{v}}-K\left(\varphi-\beta\varepsilon_{\mathrm{v}}^{\mathrm{v}}-\varphi_0\right)\mathrm{d}\varepsilon_{\mathrm{v}}^{\mathrm{v}}\\
&\quad+2G\left(e_{ij}-e_{ij}^{\mathrm{v}}\right)\mathrm{d}e_{ij}^{\mathrm{v}}-\chi_{ij}\left(\varphi-\beta\varepsilon_{\mathrm{v}}^{\mathrm{v}}-\varphi_0\right)\mathrm{d}e_{ij}^{\mathrm{v}}\\
&\quad-\chi_{ij}\left(e_{ij}-e_{ij}^{\mathrm{v}}\right)\beta\mathrm{d}\varepsilon_{\mathrm{v}}^{\mathrm{v}}-P_{\mathrm{L}}\left(b^{\mathrm{C}}+b^{\mathrm{L}}\right)\mathrm{d}\varepsilon_{\mathrm{v}}^{\mathrm{v}}+\frac{\beta}{2}P_{\mathrm{L}}\mathrm{d}\varepsilon_{\mathrm{v}}^{\mathrm{v}}\\
&\quad+(K+\chi)\left(\varphi-\beta\varepsilon_{\mathrm{v}}^{\mathrm{v}}-\varphi_0\right)\beta\mathrm{d}\varepsilon_{\mathrm{v}}^{\mathrm{v}}+\frac{\gamma_{\mathrm{CL}}}{r_P-\delta}\left(\mathrm{d}\varphi_{\mathrm{C}}+\mathrm{d}\varphi_{\mathrm{C}}^{\mathrm{v}}\right)\\
&\quad-\kappa\varepsilon_{\mathrm{v}}^{\mathrm{v}}\mathrm{d}\varepsilon_{\mathrm{v}}^{\mathrm{v}}-2\varsigma e_{ij}^{\mathrm{v}}\mathrm{d}e.
\end{aligned}
$$

As NaCl is a pure ionic crystal, the crystal deformation caused by the stress field can be small enough to be ignored. Therefore, Eq. (1) is written as:

$$
\begin{aligned}
&\sigma_m\mathrm{d}\varepsilon_{\mathrm{v}}+s_{ij}\mathrm{d}e_{ij}+P_{\mathrm{C}}\mathrm{d}\varphi_{\mathrm{C}}+P_{\mathrm{L}}\mathrm{d}\varphi_{\mathrm{L}}+\gamma_{\mathrm{SL}}\mathrm{d}A-\mathrm{d}F_{\mathrm{s}}\\
&=\left(\sigma_m+\beta P_{\mathrm{L}}+\frac{\gamma_{\mathrm{SL}}}{r_{\mathrm{P}}}\beta-\kappa\varepsilon_{\mathrm{v}}^{\mathrm{v}}\right)\mathrm{d}\varepsilon_{\mathrm{v}}^{\mathrm{v}}+\left(s_{ij}-2\varsigma e_{ij}^{\mathrm{v}}\right)\mathrm{d}e_{ij}^{\mathrm{v}}.
\end{aligned}
$$

Appendix D: Determination of P_{L} and P_{S} in Sect. 4.1

In the creep tests, the stress field is $\sigma_3 = 5$ MPa, $\sigma_1 - \sigma_3 = 10$ MPa, and the initial liquid pressure in the sandstone is $P_{\mathrm{L}}^0 = 0$, so:

$$P_{\mathrm{L}} = B^{'}\cdot\sigma_m = 0.2068 \times (15 + 5 + 5)/3 = 1.7233 \text{ MPa},$$

and

$$
\begin{aligned}
P_{\mathrm{S}}=&\frac{1}{2\pi}\int_0^{2\pi}\left(\cos^2\alpha_1\cdot\sin^2\phi_1\cdot\sigma_1+\cos^2\alpha_2\cdot\sin^2\phi_2\cdot\sigma_2\right.\\
&\left.+\cos^2\alpha_3\cdot\sin^2\phi_3\cdot\sigma_3\right)\mathrm{d}\alpha_1\\
=&\frac{1}{3}\sigma_1+\frac{1}{3}\sigma_2+\frac{1}{3}\sigma_3\\
=&\,8.3333\,\text{MPa}.
\end{aligned}
$$

References

Adamson AW (1990) Physical Chemistry of Surfaces, 5th edn. Wiley, New York

Aharonov E, Katsman R (2009) Interaction between pressure solution and clays in stylolite development: insights from modeling. Am J Sci 309:607–632

Biot MA (1941) General theory of three-dimensional consolidation. J Appl Phys 12:155–164

Borja RI (2004) Cam-clay plasticity Part V: a mathematical framework for three-phase deformation and strain localization analyses of partially saturated porous media. Comput Methods Appl Mech Eng 193:5301–5338

Borja RI (2005) Conservation laws for three-phase partially saturated granular media. In: Schanz T (ed) Unsaturated soils: numerical and theoretical approaches. Springer, Berlin, pp 3–14

Brice L (2010) Stress-induced crystal preferred orientation in the poromechanics of in-pore crystallization. J Mech Phys Solids 58:1701–1715

Cheng AHD (1997) Material coefficients of anisotropic proelasticity. Int J Rock Mech Min 34:199–205

Cohen P (1988) The ASME Handbook on Water Technology for Thermal Systems. American Society of Mechanical Engineers, p 567

Coussy O (1995) Mechanics of Porous Continua. John Wiley & Sons, Chichester

Coussy O (2004) Poromechanics. John Wiley & Sons, Chichester

Coussy O (2007) Unsaturated poroelasticity for crystallization in pores. Comput Geotech 34:279–290

Evans IS (1970) Salt crystallization and rock weathering: a review. Rev Geomorphol Dyn 19:153–177

Flatt RJ, Scherer GW (2008) Thermodynamics of crystallization stresses in DEF. Cement Concrete Res 38:325–336

Jun S (1999) Rheological behavior of geomaterial and its engineering application. China Architecture and Building Press, Beijing (in Chinese)

Lewin SZ (1982) The mechanism of masonry decay through crystallization. In: conservation of historic stone buildings and monuments. National Academy Press, Washington, DC, pp 120–144

Niels T, Sadananda S (2004) Mechanism of concrete deterioration due to salt crystallization. Mater Charact 53:123–127

Pittman ED (1992) Relationship of porosity and permeability to various parameters derived from mercury injection-capillary pressure curves for sandstone. Bull Am Assoc Petrol Geol 76:191–198

Pruess K, Spycher N (2007) ECO2N—a fluid property module for the TOUGH2 code for studies of CO2 storage in saline aquifers. Energy Convers Manag 48:1761–1767

Scherer GW (1999) Crystallization in pores. Cement Concrete Res 29:1347–1358

Seawater desalination manual (1974) Japanese Marine Corporation, Tokyo

Taylor HFW, Famy C, Scrivener KL (2001) Delayed ettringite formation. Cement Concr Res 31:683–693

Wei C, Muraleetharan KK (2002a) A continuum theory of porous media saturated by multiple immiscible fluids: I. Linear poro-elasticity. Int J Eng Sci 40:1807–1833

Wei C, Muraleetharan KK (2002b) A continuum theory of porous media saturated by multiple immiscible fluids: II. Lagrangian description and variational structure. Int J Eng Sci 40:1835–1854

Winkler EM, Singer PC (1972) Crystallization pressure of salts in stone and concrete. Geol Soc Amer Bull 83:3509–3514

Yang S, Wei J (2004) Reservoir Physics. Petroleum Industry Press, Beijing (in Chinese)

Zeidouni M, Darvish MP, Keith D (2009) Analytical solution to evaluate salt precipitation during CO2 injection in saline aquifers. Int J Greenh Gas Con 3:600–611